Numerical evaluation of the effect of geometrical and operational parameters on thermal performance of nanofluid flow in convergent–divergent tube

Farzam Akbarzadeh Hamedani[1] · Seyed Soheil Mousavi Ajarostaghi[2] · Seyed Amin Hosseini[1]

Abstract

Generally, there are two main methods to increase the thermal performance of the heat exchanger, which include active and passive methods. Passive mode, unlike active mode, does not need external power which the heat transfer rate can be increased by utilizing changes in the flow regime or direction of the fluid path. In the present survey, numerical analysis of the effect of geometrical and operational parameters on the thermal performance of a convergent–divergent tube is done. Numerical simulations are performed using the commercial CFD code. The investigated geometrical parameters include the large and smaller diameters of the cone's wall, the pitch of the cone and the height of the roughness. Obtained results in the first section indicate that the proposed wavy geometry leads to enhanced heat transfer in the pipe. In the second section of the study, instead of pure water, two types of water-based nanofluids, including water/Al_2O_3 and water/CuO, are utilized, and the obtained results are compared with pure water. Results indicate that water/Al_2O_3 nanofluid has better thermal performance than CuO/water and especially pure water. As a result, it can be said that for water/Al_2O_3 nanofluid at low Reynolds number ($Re = 10{,}000$), the case with $\varphi = 4\%$ has 9.29% more thermal performance than pure water which has the highest thermal performance. Also, at high Reynolds number ($Re = 20{,}000$), the case with $\varphi = 5\%$ has 7.15% more thermal performance than pure water. The lowest thermal performance improvement in comparison with pure water belongs to the case with $\varphi = 2\%$ at high Reynolds number ($Re = 20{,}000$) with about 6%. Also, for water/CuO nanofluid, the case with $\varphi = 3\%$ at low Reynolds number ($Re = 10{,}000$) and the case with $\varphi = 5\%$ at high Reynolds number ($Re = 20{,}000$) have highest and lowest thermal performance improvement in comparison with pure water with 8.86% and 6.25%, respectively.

Introduction

Nowadays, fossil fuels are used extensively in various industries. Due to the lack of these energies and the loss of some of them at work as waste heat, it is necessary to find efficient methods to optimize heat transfer and make better use of these energies and prevent wasting. Heat exchangers are used in various industries, such as oil and gas refineries, automotive industry and air-conditioning.

Considering different efficient parameters, including the dimensions, size and mass of heat exchangers, and saving the initial cost of construction led to various methods to optimize heat transfer in heat exchangers. In recent years,

✉ Seyed Soheil Mousavi Ajarostaghi
s.s.mousavi@stu.nit.ac.ir

Farzam Akbarzadeh Hamedani
farzam.akbarzadeh@gmail.com

Seyed Amin Hosseini
amin.hosseini@cmu.ac.ir

[1] Department of Mechanical Engineering, Chabahar Maritime and Marine University, Chabahar, Iran

[2] Department of Mechanical Engineering, Babol Noshirvani University of Technology, Babol, Iran

researchers have made great efforts to use active and passive methods to increase heat transfer in heat exchangers.

To increase the heat transfer rate in the heat exchanger, the active method needs the external force such as surface vibration and spray, whereas the passive method does not require external power. By changing the geometry of the heat exchanger and the flow regime or by adding additives to the fluid, heat transfer rates can be increased. Due to the low cost, the use of this method has been of great interest. Passive methods are utilizing any device which produces swirl flow like twisted tape, turbulators, wire coil, and etc. On the other hand, any change in the direction of the fluid path, which increases the contact of fluid and wall with constant heat flux, is a passive method. In the recent years, there are a huge number of published studies which are related to passive methods of heat transfer enhancement. Some of them are listed as follows.

Rainieri and Pagliarini [1] studied experimentally the effect of utilizing a corrugated tube in heat transfer enhancement of the double-pipe heat exchanger. The range of considered Reynolds number was between 90 and 800. Two different corrugation patterns, including axial symmetrical and helical corrugations, were tested. Results indicated that the geometry and pattern of corrugation have a significant effect on local Nusselt number. Also, the helical corrugation, in comparison with the other, makes major swirl flows and heat transfer enhancement. Promvonge and Eiamsa-ard [2] utilized two passive techniques, including conical ring and twisted tape turbulators, experimentally to enhance the heat transfer in a double-pipe heat exchanger. The range of considered Reynolds number is between 6000 and 26,000. The results showed that the average heat transfer rate increased by about 367% in comparison with plain tube. Also, the friction factor raised extensively. Garcia et al. [3] studied the effect of three different methods of synthetic roughness on the improvement of heat transfer rate. The results showed that for Reynolds number less than 200, the application of flat tubes, for Reynolds between 200 and 2000, the use of coils, and for Reynolds above 2000, using tubes, result in a better thermal performance.

The increase in heat transfer was experimentally studied by Eiamsa-ard et al. [4] using three spiral tube strips (HTTs). These experiments were carried out for Reynolds number between 6000 and 20,000. The results indicated that the highest thermal performance coefficient of 1.29 was obtained using the tape having the largest ratio of the bolt in Reynolds number 6000. Rabienataj et al. [5] investigated the turbulent heat transfer numerically once by aluminum oxide nanofluid and again by pure water inside the curved spiral tubes. The study was performed in Reynolds number between 10,000 and 40,000. The results showed that adding 2% and 4% nanoparticles to water increased heat transfer by 21% and 58%, respectively.

Mohammadi and Sabzpooshani [6] conducted an investigation in parametric performance and increasing the air heating using fin and baffle. In the utilized method, because of the reduction of the flow path and the consequent reduction of the hydraulic diameter, the heat transfer rate rises by breaking in fluid flow and forming secondary flows in a heat exchanger.

Naik et al. [7] compared the thermal performance of utilizing twisted tapes and coil in turbulence nanofluid of CuO/water experimentally. Results indicated that the thermal conductivity related to the nanofluid in a pipe with coil was higher than that observed in a pipe with twisted tapes. Esmaeilzadeh et al. [8] investigated the application of the twisted tape to increase heat transfer. Their results claim that the twisted tapes have a significant effect on the increase of heat transfer and also the friction factor since the twisted tapes enforce the degree of turbulence.

The thermal transfer characteristics and pressure drop of turbulence flow in a pipe with outer wound twisted wire were studied by Zohir et al. [9]. Experimental results showed that the heat transfer rate increases by increasing the pitch of twisted wire. Kareem et al. [10] studied the heat transfer process in a three-edge spiral wound tube experimentally and numerically. Results concluded that the increase in the heat transfer rate was 7.2–4.7 times more than the smooth tube and significant increase in friction was observed 2.4–1.7–1.5 times more than the smooth tube.

Bhuiya et al. [11] studied the heat transfer in a circular pipe with double twisted tape with opposite direction. The air is used as working fluid. The improvement of thermal efficiency in a tube with double twisted tapes with holes in a constant blower power reached about 1.08–1.44.

Afsharpanah et al. [12] performed a three-dimensional numerical simulation to study the heat transfer enhancements in a tube with double-sided twisted tape and convergent–divergent outer wall. A fixed uniform heat flux was used on the outer wall of the pipe, and water was working fluid. The geometrical parameters of the convergent–divergent wall were not investigated, and the study just focused on the geometrical parameters of the twisted tapes. The results indicated that creating a hole on the twisted tapes has no significant effect on heat transfer generally, but the effect appeared at high Re.

In the field of simulation of nanofluid by single-phase model, there are significant researches which some of them are noted as follows. Nakhchi and Esfahani [13] analyzed entropy generation for the Cu–water nanofluid flow through a heat exchanger tube equipped with perforated conical rings. Frictional and thermal entropy generation rates were defined as functions of velocity and temperature

gradients. The results indicated that the thermal irreversibility is dominant in most of the tube. But it decreases with the increase in nanoparticle volume fraction. Frictional entropy generation reduces with the increase in the number of holes from 4 to 10. Toghraie et al. [14] investigated the flow and heat transfer characteristics in smooth, sinusoidal and zigzag-shaped microchannel with and without nanofluid. Zigzag and sinusoidal-shaped channels are special kinds of the convergent–divergent channel. The results showed that by increasing the volume fraction of Copper oxide nanoparticle, Nusselt numbers are increased. Obtained results showed that if only the increase in heat transfer is considered, using sinusoidal microchannels without nanoparticles is a more effective method than using nanoparticles in smooth microchannels.

Bhattacharyya et al. [15] investigated the heat transfer and fluid flow of Al_2O_3–water nanofluid in an inclined enclosure numerically. The heated side wall of the enclosure was considered to be wavy, while the top wall is made to translate horizontally. The wavy physical domain was transformed into a square computational domain through a suitable coordinate transformation. The effect of the nanoparticle bulk volume fraction and nanoparticle diameter on the mixed convection was analyzed. The inclination angle of the enclosure is found to have an impact on the mixed convection when the buoyancy force is dominant. Heat transfer augmentation occurs as the wave number, and wave amplitude of the wavy side wall is increased. Mohebbi et al. [16] performed 2D numerical simulations to study the laminar forced convection of a nanofluid in a ribbed channel with apart heating (cooling) sources using the lattice Boltzmann method (LBM). The multi-walled carbon nanotubes–iron oxide nanoparticles/water hybrid nanofluid (MWCNT–Fe_3O_4/water hybrid nanofluid) was used in this simulation. The effect of Reynolds number (Re = 25, 50, 75 and 100), nanoparticle solid volume fraction (ϕ = 0, 0.001, 0.003) and the ratio of the blocks height (A = 0.2, 0.3, 0.4) were measured. The obtained results showed a maximum value of 16.49% increase in the average heat transfer coefficient for all the considered cases relative to the base fluid. Moreover, the local Nusselt number proved that the use of blocks on the channel walls could increase the amount of heat transfer.

Sajid et al. [17] comprised experimental investigation on heat transfer and hydrodynamic characteristics of TiO_2 nanofluid as the coolant in wavy channel heat sinks having three different channel configurations. The performance of TiO_2 nanofluids having concentrations of 0.006, 0.008, 0.01 and 0.012 vol% is compared with that of distilled water under laminar regime at heating powers of 25 W, 35 W and 45 W. Results indicated that for all heat sinks, nanofluids showed better heat transfer characteristics than distilled water. With an increase in heating power, TiO_2

nanofluid thermal performance was decreased. Kuppusamy et al. [18] performed a numerical investigation to study the thermal and flow fields in a trapezoidal grooved microchannel heat sink (TGMCHS) using nanofluids. The influence of the geometrical parameters such as the width, depth and the pitch of the groove on the thermal performance of TGMCHS was examined. The considered nanofluid is Al_2O_3–H_2O. Results indicated that Al_2O_3–H_2O had the highest thermal performance with 0.04 volume fraction and 25 nm particle diameter.

Kuppusamy et al. [19] conducted a numerical simulation to examine the heat transfer and fluid flow characteristics of nanofluids in a triangular grooved microchannel heat sink (TGMCHS). The effect of the geometrical parameters such as the angle (50–100°), depth (10–25 μm) and the pitch (400–550 μm) of the groove on the thermal performance of TGMCHS was examined. The effects of different nanoparticle types (Al_2O_3, CuO, SiO_2, ZnO), volume fraction (Ø = 0.01–Ø = 0.04), particle diameter (25–80 nm) and base fluid (water, ethylene glycol, engine oil) at different Reynolds numbers are also studied. It is found that the TGMCHS thermal performance of using Al_2O_3–H_2O (Ø = 0.04, d_{np} = 25 nm) is outperformed the simple MCHS using water. Mohammed and Narrein [20] investigated numerically the effects of using different geometrical parameters with the combination of nanofluid on heat transfer and fluid flow characteristics in a helically coiled tube heat exchanger. A CuO nanoparticle with a diameter of 25 nm dispersed in water with a particle concentration of 4% was used as the working fluid. The results revealed that certain geometrical parameters such as the helix radius and inner tube diameter do affect the performance of the HCTHE under laminar flow conditions. It was also found that counter-flow configuration produced better results as compared to parallel-flow configuration.

Narrein and Mohammed [21] studied the effects of using various types of nanofluids and rotation on heat transfer and fluid flow characteristics in a helically coiled tube heat exchanger numerically. Mainly, the effects of nanoparticles type (Al_2O_3, SiO_2, CuO, ZnO), its concentration (1–4%) and particle diameter (25–80 nm), and base fluid type (water, ethylene glycol, engine oil), toward the heat transfer and fluid flow characteristics, are comprehensively analyzed. The results revealed that nanofluids could enhance the thermal properties and performance of the HCTHE, but it was accompanied by a slight increase in pressure drop. It was found that the Nusselt number is highest using CuO–water nanofluid in this study. Also, rotation can be used to enhance the heat transfer rates. Mohammed et al. [22] evaluated the effects of two-dimensional laminar and turbulent combined convection nanofluids flow over backward-facing step in a channel having a blockage, numerically. The duct has a step height

of 0.01, and an expansion ratio of 2. The Reynolds number was in the range of 100–1900 (laminar flow) and in the range of 4000–10,000 (turbulent flow). The effect of the blockage shape (circular, square and triangular) on the flow and heat transfer characteristics is examined. The effects of various types of nanoparticles such as Al_2O_3, SiO_2, CuO and ZnO dispersed in a base fluid (water), the volume fraction of nanoparticles in the range of 1–4% and nanoparticle diameter in the range of 25–80 nm were also studied.

In this survey, a numerical study of the effect of geometric parameters on the performance of double-tube heat exchangers with a convergent–divergent tube is carried out numerically. A commercial CFD code, ANSYS FLUENT 18.2 software, was utilized to perform numerical simulations. The effect of four geometrical parameters, including the large and smaller diameters of the cone's wall, the pitch of the cone and the height of the roughness and the flow parameter (Reynolds number) has been investigated and analyzed. At the second section of the study, instead of pure water, two types of water-based nanofluids, including water/Al_2O_3 and water/CuO are utilized, and the obtained results are compared with pure water.

Novelty of present paper In the previous studies, change in the geometry of the channel to increase the heat transfer enhancement has been an efficient method as a passive method. Among different kinds of channel's wall like corrugated, zigzag, sinusoidal and, etc., the convergent–divergent tube is a new geometric for the channel which causes high heat transfer rate in comparison with the simple tube. In the present paper, the numerical simulations are performed to investigate the effects of the geometrical and operational parameters of the convergent–divergent tube. Also, in the second section of the present study, as well as water, two water-based nanofluids, including water/Al_2O_3 and water/CuO, are considered and analyzed as working fluid. In the third section of the present study, the effect of different volume concentrations of the water-based nanofluid on heat transfer enhancement is investigated. The present study is the first comprehensive article which focuses just on heat transfer enhancement in a convergent–divergent tube.

Research method, calculations and formulas

Here, the general form of the governing equations is presented first. Three-dimensional equations governing the mass conservation, momentum and energy were solved utilizing the computational fluid dynamic.

Single-phase equations consist of mass, momentum and energy equations. Momentum and mass conservation equations are applied to calculate velocity vectors. The temperature distribution and the heat transfer coefficient of the wall are computed with the energy equation. The equations for the conservation of mass, momentum and energy are as follows [23]:

Mass conservation equation

Mass conservation equation or continuity is as follows:

$$\frac{\partial \rho}{\partial t} + \nabla \nabla \cdot (\rho \vec{v}) = S_m \tag{1}$$

Equation 1 is the general form of mass conservation equation, which is valid in compressible and incompressible flows. The mass added to the continuous phase of the second phase of the diffusion is defined like the evaporation of liquid droplets or any other defined source.

Momentum conservation equation

Momentum conservation equation in any non-accelerated coordinate system is defined as follows:

$$\frac{\partial (\rho \vec{v})}{\partial t} + \nabla \cdot (\rho \vec{v} \vec{v}) = -\nabla p + \nabla (\overline{\overline{\tau}}) + \rho \vec{g} + \vec{F} \tag{2}$$

where P is the static pressure, $\overline{\overline{\tau}}$ is the stress tensor and $\rho \vec{g}$ and $\vec{F}$ are the volumetric forces of acceleration of gravity and involved foreign forces. The tension tensor is defined as:

$$\overline{\overline{\tau}} = \mu \left[\left(\nabla \vec{v} + \nabla \vec{v}^T - \frac{2}{3} \nabla \cdot \vec{v} I \right) \right] \tag{3}$$

where in the above relation, μ is the molecular viscosity, I is the tensor, the second term to the right is the volume change effect. To perform numerical computations, there are many turbulent modeling methods. Realizable k-ε model is one of the two-equation models for turbulent modeling presented by shih et al. [24], which is utilized here to model the turbulent fluid flow and heat transfer. For boundary condition: at the outer wall, no-slip boundary condition and constant wall heat flux were applied, and in the flow inlet boundary, constant velocity and constant temperature were assumed.

Energy conservation equation

Energy equation defined below:

$$\begin{aligned} \frac{\partial (\rho E)}{\partial t} + \nabla \cdot (\vec{v}(\rho E + p)) \\ = \nabla \left(k_{eff} \nabla T - \sum_j h_j \vec{J}_j + (\overline{\overline{\tau}}_{eff} \cdot \vec{v}) \right) + S_h \end{aligned} \tag{4}$$

where k is the thermal conductivity and $\vec{J}_j$ is the diffusion flux of different kinds. The three first-order terms to the right of Eq. 4 are guidance, diffusion and loss of viscosity,

respectively. S_h consists of heat generated by chemical reactions or any other volume heating source.

Thermophysical properties of nanofluid

Addition of nanoparticle to the water can improve the thermophysical properties of it. Many experimental measurements have been done to obtain the properties of nanofluid and the results show that changes in viscosity and thermal conductivity of nanofluid do not carry out the mixture rules, so several researchers suggested different correlations to predict the thermophysical properties. The effective properties of nanofluid are defined as follows:

Density [25]:

$$\rho_{nf} = (1 - \phi)\rho_f + \phi\rho_{np} \tag{5}$$

Specific heat capacity [26]:

$$C_{P_{nf}} = \frac{(1 - \phi)(\rho C_{np})_f + \phi(\rho C_{np})_{np}}{\rho_{nf}} \tag{6}$$

Thermal conductivity [27]:

$$\frac{k_{nf}}{k_f} = 1 + 4.4 Re^{0.4} Pr^{0.66} \left(\frac{T}{T_{fr}}\right)^{10} \left(\frac{k_{np}}{k_f}\right)^{0.03} \phi^{0.66} \tag{7}$$

where Re is the nanofluid Reynolds number, Pr is the Prandtl number of base fluid, T is nanofluid temperature, T_{fr} is the freezing point of the base fluid, k_P, and ϕ are thermal conductivity and the volume concentration of the nanoparticle, respectively.

Viscosity [28]:

$$\frac{\mu_{nf}}{\mu_f} = (1 + \phi)^{11.3} \left(1 + \frac{T - 273.15}{70}\right)^{-0.038} \left(1 + \frac{d_{np} \times 10^9}{170}\right)^{-0.061} \tag{8}$$

The water-based Al_2O_3 and CuO nanofluids are chosen in this study. The thermophysical properties of nanoparticles that are used in present simulation are shown in Table 1.

Operational parameter definition

To analysis the results, some parameters, including the non-dimensional numbers, are necessary that will be as follows:

Reynolds number:

$$Re = \frac{\rho u d_h}{\mu} \tag{9}$$

where d_h is the hydraulic diameter.

Nusselt number:

$$Nu = \frac{h_m d_h}{k} \tag{10}$$

where h_m is the mean heat transfer coefficient:

$$h_m = \frac{\dot{q}_m}{T_w - T_m} \tag{11}$$

Mean temperature (T_m) inside the computational domain in Eq. 6 is obtained from the following equation:

$$T_m = \frac{\int_{A_{cs}} uT dA}{\int_{A_{cs}} u dA} \tag{12}$$

Friction factor:

$$f = \frac{2 d_h \Delta P}{\rho u^2 L} \tag{13}$$

Usually, a parameter as thermal performance (η) is used to evaluate the performance of the heat exchanger, which shows the effect of improving the heat transfer under known pumping power. This parameter is defined by [31–38]:

$$\eta = \left(\frac{Nu}{Nu_0}\right)\left(\frac{f_0}{f}\right)^{\frac{1}{3}} \tag{14}$$

Geometrical dimensionless parameters definition

Four different geometrical dimensionless parameters are defined here, including α_1, α_2, α_3 and α_4, which are related to large diameter of the conical wall (D_2), small diameter of the conical wall (D_1), the pitch of the convergent–divergent wall (P) and gap between two consecutive convergent–divergent sections (K), respectively. These geometrical parameters are defined as follows:

$$\alpha_1 = D_1/L \tag{15}$$
$$\alpha_2 = D_2/L \tag{16}$$

Table 1 Nanoparticle thermophysical properties

Nanoparticle	d_{np}/nm	k_{np}/W m^{-1} K	ρ_{np}/kg m^{-3}	C_{np}/J/kg K	Ref.
Al_2O_3	35	36	3880	773	[29]
CuO	29	69	6350	535	[30]

$$\alpha_3 = P/L \tag{17}$$

$$\alpha_4 = K/L \tag{18}$$

Discussion and conclusion

The studied model

The schematic of the studied model is shown in Fig. 1. Accordingly, the incoming water at 303 K enters the computational domain and collides with a convergent–divergent wall with a constant flux of 500,000 W m^{-2}.

In this paper, the effect of four geometric parameters, including small and large diameters of convergent–divergent wall, wall step and wall roughness, and the influence of Reynolds numbers in the range of 10,000–200,000, has been studied. The considered geometric and flow parameters are listed in Table 2.

In the present study, a tube with convergent–divergent outer wall (Fig. 1) is considered. The geometrical and operational parameters are investigated numerically. A comprehensive study is done to analyze the effect of geometrical parameters, including small diameter of the conical area (D_1), large diameter of the conical area (D_2), the pitch of the convergent–divergent wall (P) and the gap between two consecutive convergent–divergent sections (K). The simulations are performed in the range of Re between 100,000 and 200,000.

The numerical procedure and boundary conditions

Numerical simulation was done by using commercial CFD software ANSYS FLUENT 18.2. Governing equations with relevant boundary conditions were discretized by a finite volume method. The discretization of the momentum, turbulent kinetic energy, turbulent dissipation rate and the energy equations were performed by the second-order upwind scheme. Also, the coupling between the pressure and velocity is provided by the SIMPLE algorithm. To evaluate the variation of conductivity and viscosity with temperature, user-defined functions (UDFs) were connected to the fluid properties panel and the changes in conductivity and viscosity for all mesh elements after every iteration was implemented.

In the studied heat exchanger, the cold fluid enters into the internal tube at 80 °C with four Reynolds numbers of 10,000, 12,500, 15,000, 17,500 and 20,000. The flow is completely turbulent. The constant heat flux is considered at the wall of the tube. The VELOCITY INLET and PRESSURE OUTLET types are set as boundary conditions for inlet and outlet sections, respectively.

Validation and grid independency studies

Utilizing convergent–divergent wall to enhance the heat transfer was presented and studied firstly by Afsharpanah et al. [12]. However, they did not investigate the effect of geometrical parameters of this type of wall. The obtained results from the reference study [12] are considered to validate with the present numerical model. Nusselt number and friction coefficient versus different Reynolds numbers of inlet flow obtained from the present study are compared and indicated with the results of the reference study [12] in Fig. 2a, b, respectively. Accordingly, it can be seen that the present numerical simulations have considerable accuracy and the present numerical results have good agreement with the results from the reference study [12].

To study the effect of the size of the grid on the obtained results from numerical simulations, four different grids are considered here with 928,404, 1,318,114, 1,818,973 and 2,326,377 cells. Two parameters, including outlet temperature of channel and pressure drop versus four different Reynolds numbers for various grids, are illustrated in Fig. 3a, b, respectively.

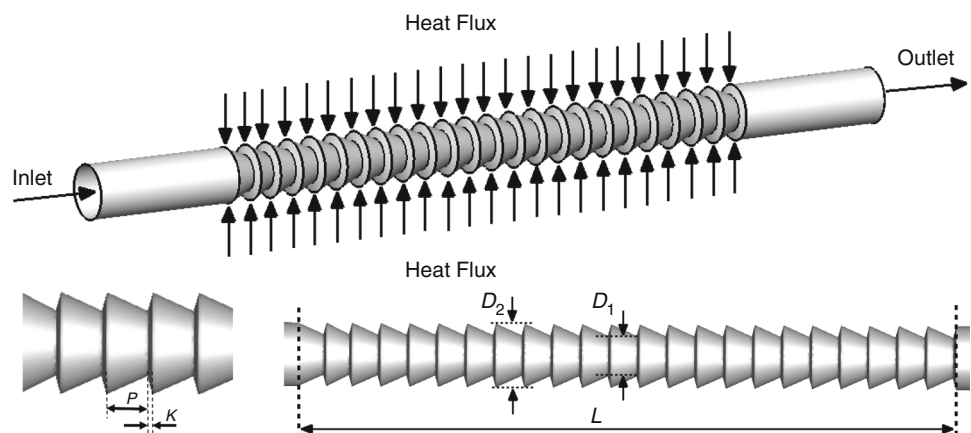Fig. 1 The schematic of the considered model with geometrical parameters

Table 2 Geometric and flow parameters of the investigated model

Parameter		Value
Geometrical parameters		
Length of the computational domain/mm	L	255.75
Small diameter of the conical area/mm	D_1	16–18–20–22
Large diameter of the conical area/mm	D_2	19–21–23–25
Pitch of the convergent–divergent wall/mm	P	8–12–12–14
Gap between two consecutive convergent–divergent sections/mm	K	1.75–1.5–1.25–1
Flow parameters		
Inlet temperature of water/K	T_{inlet}	303
Inlet Reynolds number/Re	Re	10,000–20,000
Heat flux of the convergent–divergent wall/W m^{-2}	$\ddot{Q}$	500,000
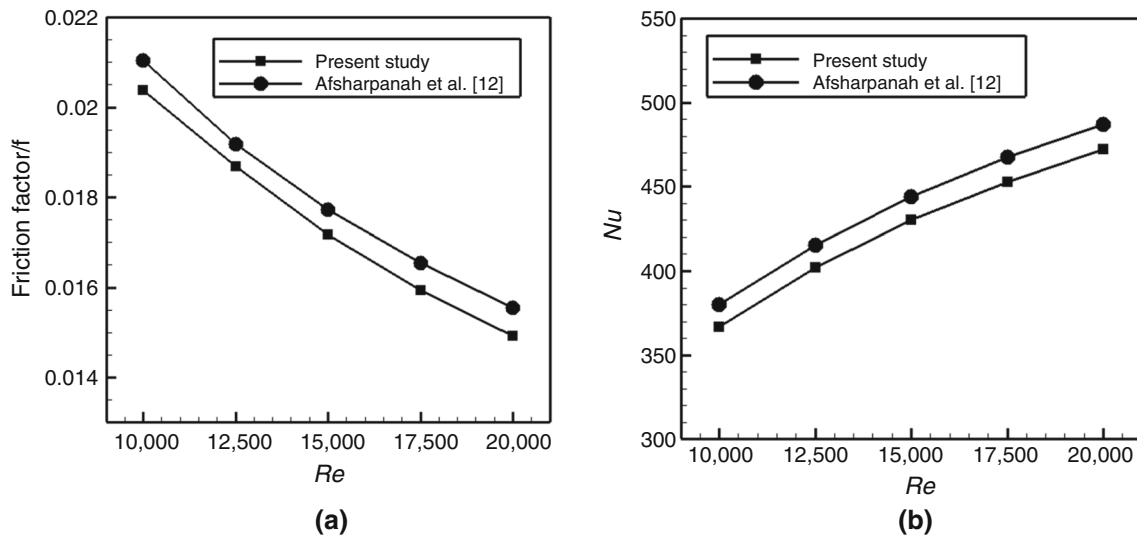
Fig. 2 Validation of the present numerical study with the results of the reference study [12] **a** Nusselt number versus *Re* and **b** friction coefficient versus *Re*

According to Fig. 3a, b, there is no significant difference in the results obtained for two grids of 1,818,973 and 2,326,377 cells. So, to decrease the computational cost and time, grid with 1,818,973 cells is selected for performing numerical simulations. The schematic of the generated grid in the tube and outer wall of the tube is illustrated in Fig. 4.

The effect of dimensionless geometrical parameter of α_1 (large diameter of the conical area (D_2))

In this part, the effect of the large diameter of the conical area (D_2) on heat transfer and fluid flow is analyzed numerically. The small diameter of the conical area (D_1), the pitch of the convergent–divergent wall (P) and the gap between two consecutive convergent–divergent sections (k) are kept constant as 18 mm, 10 mm and 1.25 mm, respectively. The other constant operational and geometrical parameters of the considered geometry are listed in Table 1.

Four different values are considered for large diameter of the conical area (D_2), including 19, 21, 23 and 25 mm. The outlet temperature of water and the pressure drop in the tube are illustrated in Fig. 5a, b, respectively.

Figure 5a indicates that the temperature of output water decreases as Reynolds number increases and this reduction is visible to all models. Also, Fig. 5a shows that as the diameter of the cone wall increases, the temperature of the outlet water from the converter increases.

About the pressure drop, Fig. 5b indicates that the pressure drop increases as Reynolds number rises, and this increase is shown for all models. On the other hand, the trend of Fig. 5a, b is the same for all models. Because, it is also worth noting that growing the large diameter of the cone increases the pressure drop.

The contours of temperature are drawn on a plate in the middle of the channel for a large diameter of the cone of different models in Fig. 6. Accordingly, by increasing the large diameter of the cone, the temperature of water reaches a better output and is a better temperature
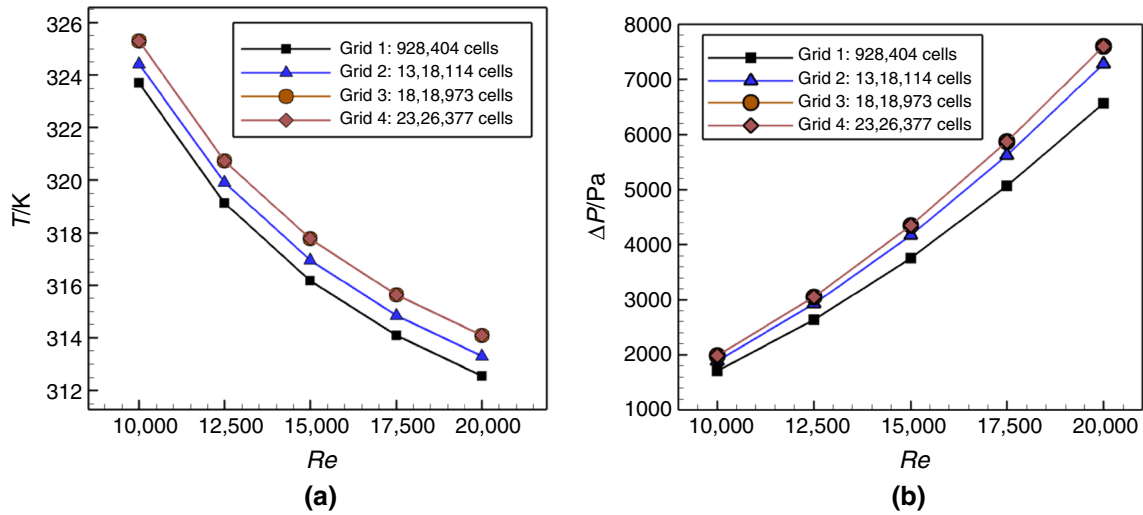
Fig. 3 Mesh independency study **a** outlet temperature of the channel and **b** pressure drop versus different Reynolds numbers for four various grids
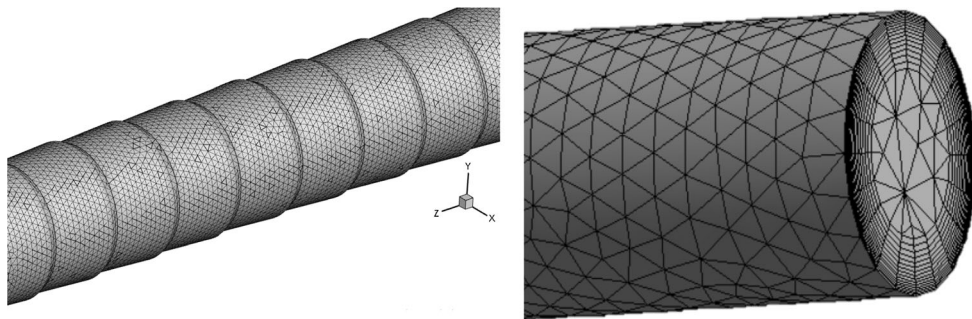

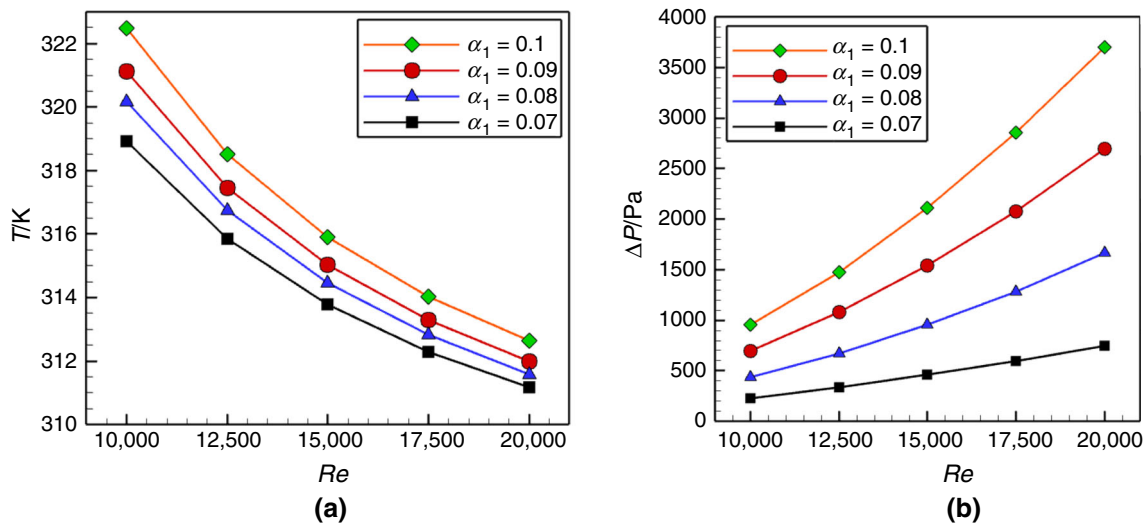**Fig. 4** The schematic of the generated grid for considered geometry

Fig. 5 **a** Outlet temperature of water versus Reynolds number and **b** pressure drop versus Reynolds number for $D_1 = 18$ mm, $P = 10$ mm and $K = 1.25$ mm

uniformity observed on the plate. Also, based on the contours plotted in Fig. 6, it can be concluded that the best temperature of outlet water and best temperature uniformity are achieved in the large diameter of 25 mm. The contours of temperature in the outlet of channel are shown in Fig. 7 for various large diameters of the cone. Accordingly, for a large diameter of the cone, as the same as obtained results in Fig. 6, a higher temperature uniformity at the outlet of channel can be seen, with a large diameter of 25 mm.

The average Nusselt number versus different Reynolds numbers of inlet flow is illustrated in Fig. 8a. Accordingly, it can be seen that because of the force convection, as the Reynolds number rises, the average Nusselt number (Nu) increases for all models. Also, as a constant Re, by increasing the large diameter of the conical area (D_2), the Nusselt number rises which the trend is the same for all investigated Re.

To analysis the both of heat transfer and pressure drop in the computational domain, a parameter as thermal performance is defined as Eq. 14 which the f_0 and Nu_0 are referred to the case with $\alpha_1 = 0.07$ ($D_2 = 19$ mm). The thermal performance of the computational domain versus with different Re is illustrated in Fig. 8b for various models. Accordingly, the thermal performance of the $\alpha_1 = 0.07$ is equal to unity (base model). It can be seen that as the α_1 dimensionless geometrical parameter or large diameter of the conical area (D_2) increases (more than the base model: $\alpha_1 = 0.07$ ($D_2 = 19$ mm)), the thermal performance declines (lower than unity) which means that high large diameter of the conical area (D_2) leads to the low

thermal performance although the more heat transfer rate belongs to higher α_1 (D_2) according to Fig. 8a.

As a result, in this section, by increasing the α_1 dimensionless geometrical parameter or large diameter of the cone (D_2), better temperature uniformity, or a better heat transfer between the wall and the fluid occurs. Therefore, it can be concluded that the large diameter increase will have a significant effect on the temperature of the water output from the converter. However, according to Fig. 5b, the more pressure drop belongs to the case with higher α_1 (or D_2). So, it affects the thermal performance parameter (η) and highest thermal performance is obtained at lowest α_1 (or D_2) based on Fig. 8b.

Because of the very low slope of the profiles in Fig. 8b, the values of thermal performance for different models and Reynolds numbers are listed in Table 3. According to Fig. 8b and Table 3, the highest thermal performance belongs to the case with $\alpha_1 = 0.07$ ($D_2 = 19$ mm) in all considered Reynolds number and the lowest one belongs to the case with $\alpha_1 = 0.01$ ($D_2 = 25$ mm) at $Re = 10,000$ which is not clear in Fig. 8b.

It should be noted according to Sect. 3.4, the case with $\alpha_1 = 0.07$ schematically is very close to simple tube. So, as the α_1 dimensionless geometrical parameter increases, the convergent–divergent tube shows its effect significantly and according to Fig. 8a, average Nusselt number rises which shows higher heat transfer rate. At low Reynolds number ($Re = 10,000$), the average Nusselt number of the case with $\alpha_1 = 0.1$ is 30.55% more than the case with $\alpha_1 = 0.07$ (like simple tube). At high Reynolds number ($Re = 20,000$), the average Nusselt number of the case with
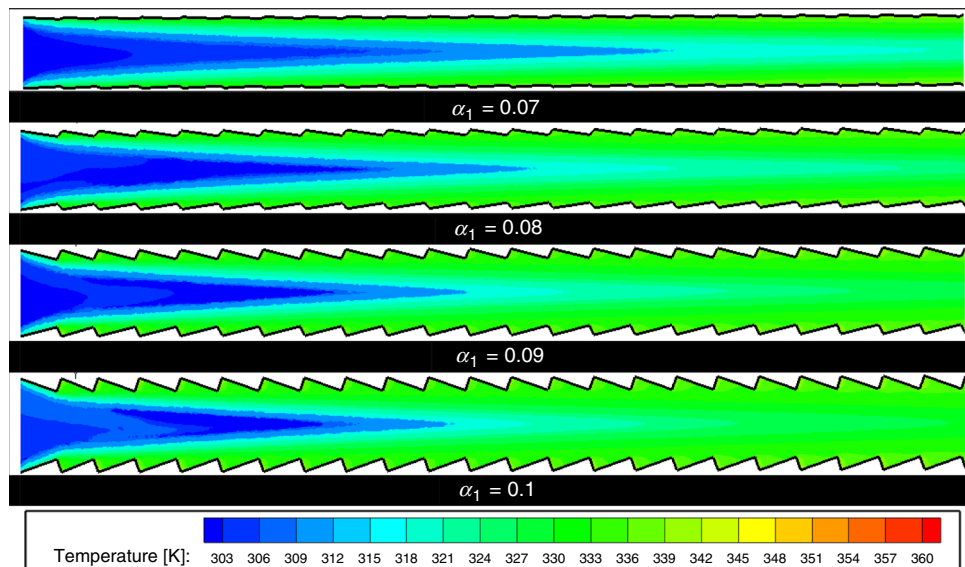

Fig. 6 The contours of temperature in the middle of the channel for $Re = 15,000$, $D_1 = 18$ mm, $P = 10$ mm and $K = 1.25$ mm
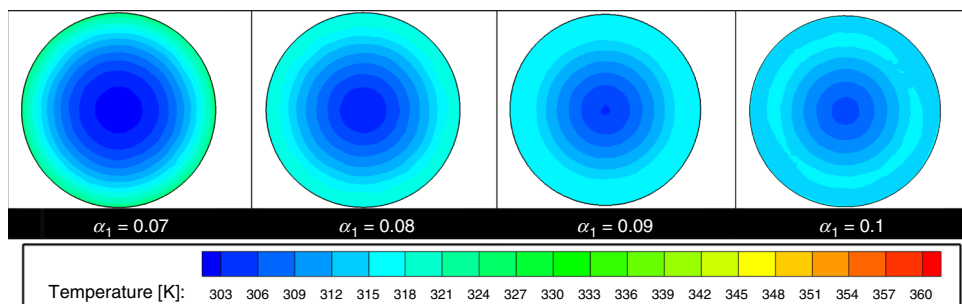
Fig. 7 Contours of temperature at the outlet of tube for Re = 15,000, D_1 = 18 mm, P = 10 mm and K = 1.25 mm
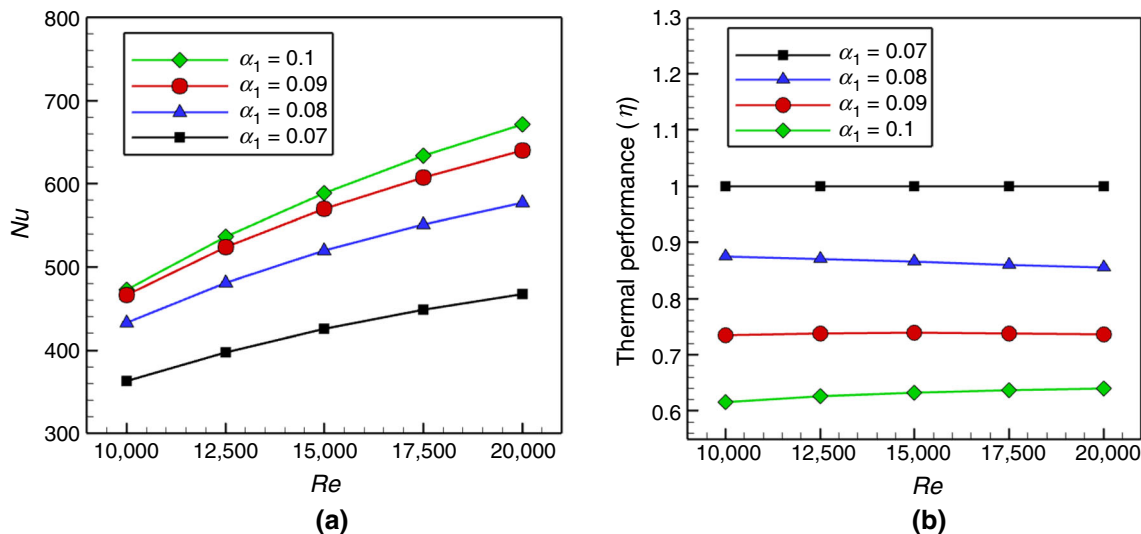

Fig. 8 a Average Nusselt number (Nu) and **b** thermal performance (η) versus Reynolds number different α_1 dimensionless parameters (different large diameters of the cone) at D_1 = 18 mm, P = 10 mm and K = 1.25 mm

α_1 = 0.1 is 42.55% more than the case with α_1 = 0.07 (like simple tube).

As the Reynolds number increases, the heat transfer enhancement rises more. Also, Fig. 8b shows that as the α_1 dimensionless geometrical parameter increases, the thermal performance declines because of the high pressure drop at higher α_1.

In Fig. 9, 3D streamline with contour of velocity magnitude for two different α_1 dimensionless geometrical parameters, including α_1 = 0.07 and 0.1 at Re = 20,000, is shown. Accordingly, it can be seen that at α_1 = 0.07, the

effect of the geometry of the tube is lower than the case with α_1 = 0.1. On the other hand, at α_1 = 0.07, there are no secondary flows in the connection of convergent and divergent parts of the tube. However, at α_1 = 0.1, there are vortexes and secondary flows clearly in the connection of convergent and divergent parts of the tube which affect the heat transfer rate significantly.

The effect of dimensionless geometrical parameter of α_2 (small diameter of the conical area (D_1))

In this section, the influence of dimensionless geometrical parameter of α_2 (or the small diameter of the cone (D_1)) on the temperature of the outlet water and the drop in the pressure of the outlet water are analyzed numerically. In this study, the large diameter of the cone (D_2) is kept constant as 25 mm (α_1 = 0.1).

The temperature of output water and pressure drop versus Reynolds numbers for different models (different values of the small diameter of the cone) are shown in

Table 3 Thermal performance (η) for different α_1 and Re

Re	α_1 = 0.07	α_1 = 0.08	α_1 = 0.09	α_1 = 0.1
10,000	1	0.874	0.735	0.616
12,500	1	0.87	0.738	0.626
15,000	1	0.865	0.739	0.632
17,500	1	0.86	0.738	0.637
20,000	1	0.855	0.736	0.639

Fig. 10a, b, respectively. In this section, the large diameter of the cone is kept constant as 25 mm ($\alpha_1 = 0.1$), while the small diameter of the cone varies between 16 and 22 mm ($\alpha_2 = 0.06$–0.09).

Based on Fig. 10a, as the Reynolds number gets larger, the temperature of output water is reduced by the Reynolds number too. This reduction is seen in all models. Also, it can be seen that the temperature of the outlet water increases with the decrease in small diameter of the vapor wall cone. Accordingly, the highest temperature of outlet water belongs to the small diameter of 16 mm. In all the models presented in Fig. 10b, the pressure drop increases with the increase in the Reynolds number. It is also worth noting that reducing the small diameter of the cone increases the drop in pressure. In Fig. 11, the contours of temperature are depicted on a plate in the middle of the channel for different small diameters of the cone.

Figure 11 shows that reducing the small diameter of the cone causes the temperature of output water to increase, so that the uniformity is significant. Accordingly, small diameter of 16 mm has the highest output temperature of water and better temperature uniformity.

Figure 12 depicts the contours of temperature in the output of channel for different diameters of the small diameter of cone. As the same results in Fig. 11, the temperature uniformity is also shown by decreasing the small diameter of the cone with increasing temperature. This temperature uniformity is quite clear when comparing D_1 with a small diameter of 22 mm ($\alpha_2 = 0.09$) and a small diameter of 16 mm ($\alpha_2 = 0.06$). Therefore, at the smaller diameter of the cone, it increases the temperature and a better uniformity occurs between the wall and the fluid.

The average Nusselt number (Nu) and thermal performance (η) versus the Reynolds number of the inlet flow for various small diameter of the cone are illustrated in Fig. 13a, b, respectively. According to Fig. 13a, it can be seen that as Reynolds number (Re) rises, the average Nusselt number (Nu) increases because of the effect of
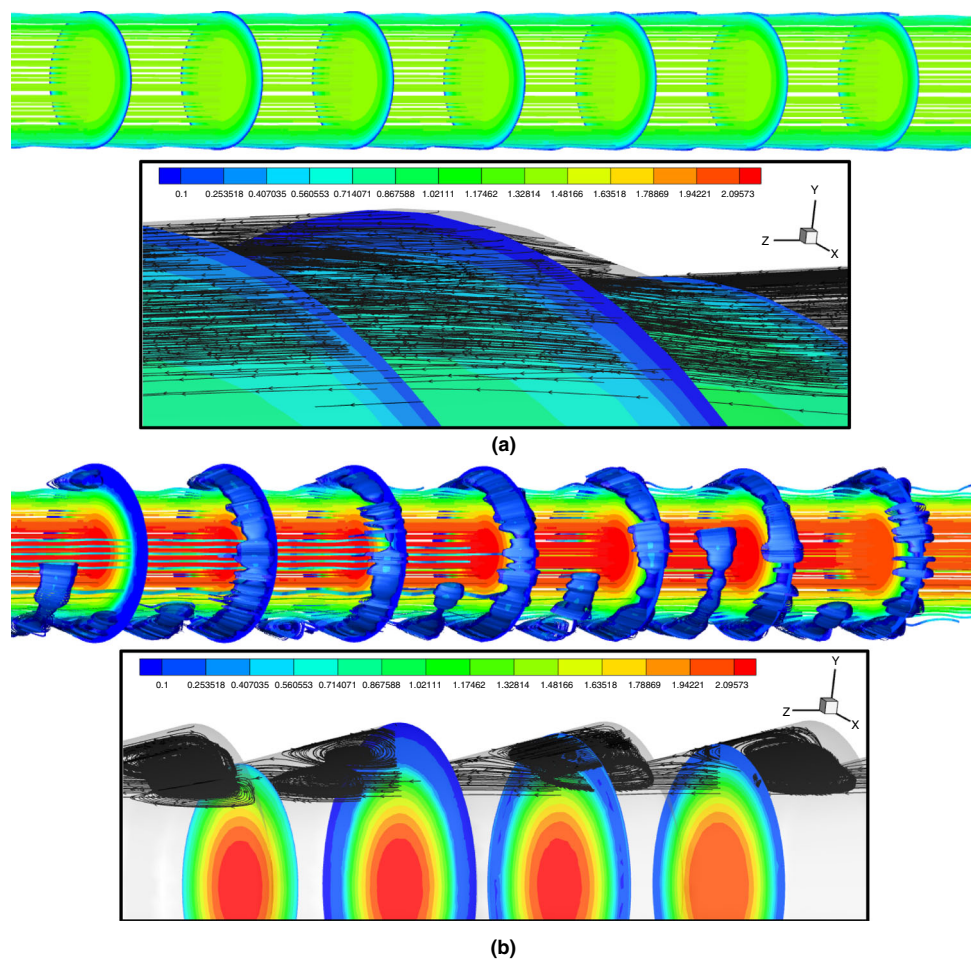

Fig. 9 Streamline with velocity magnitude (m/s) for two different α_1 dimensionless geometrical parameters at $Re = 20,000$ **a** $\alpha_1 = 0.07$ and **b** $\alpha_1 = 0.1$

force convection. Also, at a constant Re (Re = cte), by increasing the small diameter of the cone (D_1), the average Nusselt number (Nu) declines.

The thermal performance (η) versus different Reynolds numbers (Re) for various small diameter of the cone (D_1) is illustrated in Fig. 13b. The case with $D_1 = 22$ mm is the base case which the thermal performance of this case is equal to unity ($\eta = 1$) and the other models are compared with this case. Accordingly, the results show that lowest small diameter of the cone leads to higher thermal performance (high heat transfer rate with low pressure drop).

Because of the very low slope of the profiles in Fig. 13b, the values of thermal performance for different models and Reynolds numbers are listed in Table 4. According to Fig. 13b and Table 4, the highest thermal performance belongs to the case with $\alpha_2 = 0.09$ ($D_1 = 22$ mm) in all considered Reynolds number and the lowest one belongs to the case with $\alpha_2 = 0.06$ ($D_1 = 16$ mm) at $Re = 10,000$ which is not clear in Fig. 13b.

In Fig. 14, 3D local Nusselt number on the surface of the wall of tube for two different α_2 dimensionless geometrical parameters, including $\alpha_2 = 0.06$ and 0.09 at $Re = 20,000$, is shown. Accordingly, it can be seen that at $\alpha_2 = 0.06$, the effect of the geometry of the tube is higher than the case with $\alpha_2 = 0.09$. Based on Fig. 12, maximum local Nusselt number of the case with $\alpha_2 = 0.06$ is 65.25% more than maximum local Nusselt number of the case with $\alpha_2 = 0.09$.

The effect of dimensionless geometrical parameter of α_3 (pitch of the convergent–divergent wall (P))

In this section, the effect of dimensionless geometrical parameter of α_3 (or the pitch of the convergent–divergent wall (P)) on the temperature of the outlet water and the drop in the pressure of the outlet water is analyzed numerically. In the studies, the amount of α_3 of the wavy wall is differently considered as $\alpha_3 = 0.03, 0.04, 0.05$ and 0.06 (or $P = 8, 10, 12$ and 14 mm).

The output temperature of water and pressure drop versus different Reynolds numbers for various models are shown in Fig. 15a, b, respectively. Figure 15a indicates that the output water temperature decreases with Reynolds number in terms of Reynolds number, and this reduction is observed in all models. Also, as the size of the convergent–divergent wall decreases, the temperature of the outlet water rises. However, it is observed that the maximum output temperature of water belongs to the pitch of 8 mm.

According to Fig. 15b, by increasing Reynolds number, the pressure drop rises, and this trend is same for all models. Also, declining the size of the wall leads to an increase in the pressure drop. The contours of temperature are drawn on a plate in the middle of the channel to measure the different steps of different wavy walls in Fig. 16. It can be seen that by decreasing the step size, the temperature of the outlet water increases. Accordingly, the
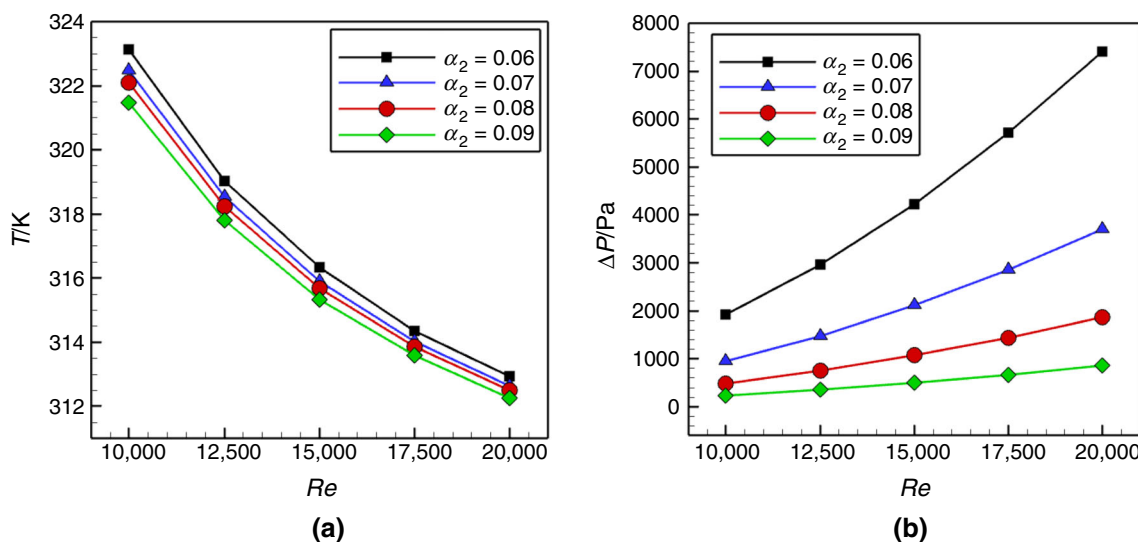

Fig. 10 a The temperature of outlet water and **b** pressure drop versus different Re for different α_2 dimensionless parameters (different small diameters of the cone) at $D_2 = 25$ mm, $P = 10$ mm and $K = 1.25$ mm
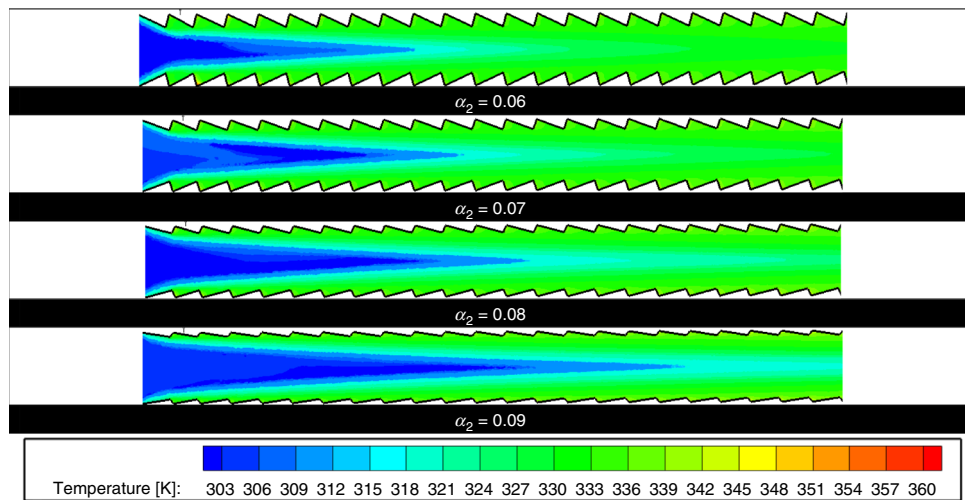
Fig. 11 The contours of temperature in the middle of the channel for different α_2 dimensionless parameters (different small diameters of the cone) at $Re = 15{,}000$, $D_2 = 25$ mm, $P = 10$ mm and $K = 1.25$ mm
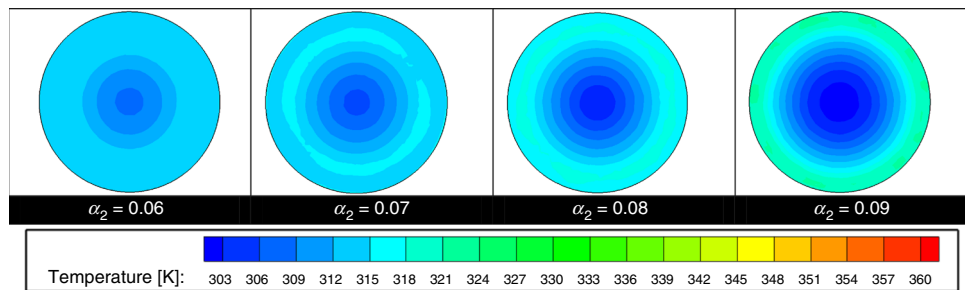

Fig. 12 Contours of temperature at the outlet of tube for different α_2 dimensionless parameters (different small diameters of the cone) at $Re = 15{,}000$, $D_2 = 25$ mm, $P = 10$ mm and $K = 1.25$ mm

best output water temperature and the best heat transfer belong to the case with $P = 8$ mm ($\alpha_3 = 0.03$).

The temperature contour at the output is depicted in Fig. 17 for various steps of the wavy wall. By reducing the size of the wavy wall step, as shown in Fig. 16, the output water temperature is a bit out of uniformity. By increasing the size of the wavy wall step, there is a better temperature uniformity between the wall and the fluid, but this temperature uniformity decreases the water output temperature. So, decreasing step size results in a higher output temperature.

The average Nusselt number (Nu) and thermal performance versus Reynolds number (Re) for various pitches of the convergent–divergent wall (P) are depicted in Fig. 18a, b, respectively. Figure 18a shows that at low Reynolds number ($Re = 10{,}000$), the difference between the calculated average Nusselt number (Nu) and the investigated models are very low. At high Reynolds number, as the pitch of the convergent–divergent wall (P) rises, the

average Nusselt number (Nu) decreases. According to Fig. 18b, the highest thermal performance is achieved for the case with $P = 8$ mm ($\alpha_3 = 0.03$).

In Fig. 18b, it should be noted that the case with $P = 14$ mm ($\alpha_3 = 0.06$) is the base case which the thermal performance is equal to unity ($\eta = 1$). Both parameters rise as the Reynolds number increases.

The effect of dimensionless geometrical parameter of α_4 (gap between two consecutive convergent–divergent sections (K))

In this section, the influence of the gap between two consecutive convergent–divergent sections (K) on the temperature of the outlet water and the drop in the pressure of the outlet water is studied numerically. Four different K, including 1, 1.25, 1.5 and 1.75 mm, are considered in this section. A dimensionless parameter related to this parameter is defined by Eq. 18 as α_4. Accordingly, four different
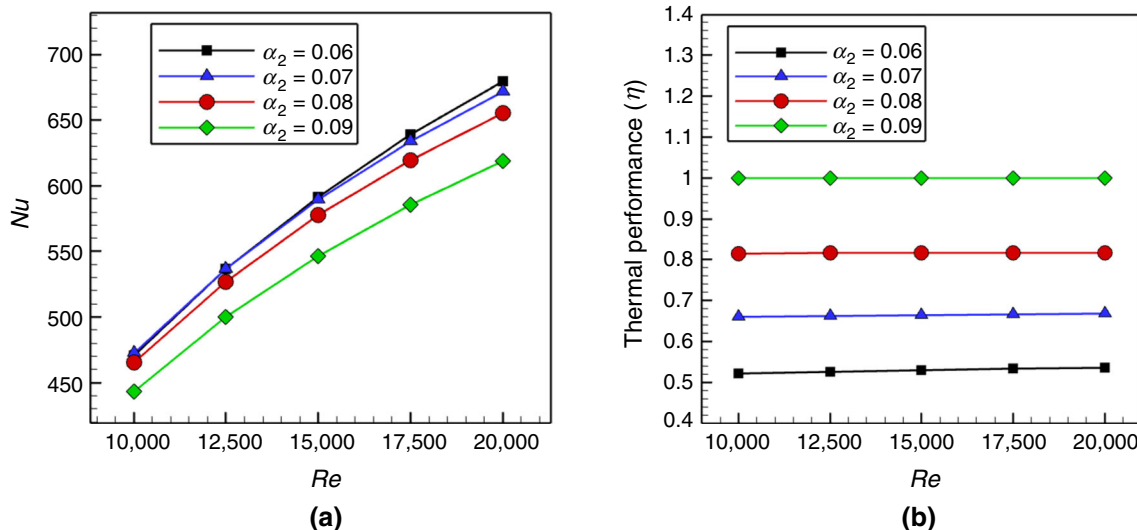
Fig. 13 **a** Average Nusselt number (Nu) and **b** thermal performance (η) versus Reynolds number for different α_2 dimensionless parameters (different small diameters of the cone) at $D_2 = 25$ mm, $P = 10$ mm and $K = 1.25$ mm

Table 4 Thermal performance (η) for different α_2 and Re

Re	$\alpha_2 = 0.06$	$\alpha_2 = 0.07$	$\alpha_2 = 0.08$	$\alpha_2 = 0.09$
10,000	0.52	0.66	0.815	1
12,500	0.526	0.662	0.816	1
15,000	0.53	0.665	0.8172	1
17,500	0.531	0.666	0.8173	1
20,000	0.535	0.667	0.8174	1

α_4 including 0.003, 0.004, 0.005 and 0.006 are utilized here.

The pressure drop and outlet temperature of the fluid versus the Reynolds number of the inlet flow for various gap between two consecutive convergent–divergent sections (K) are depicted in Fig. 19a, b, respectively.

Figure 19a shows that the differences in pressure drop between the investigated models here are so low and as Reynolds number rises, pressure drop increases. In Fig. 19b, it can be seen that as the Reynolds number increases, the output water temperature also decreases because of the effect of force convection. The trend is the same for all models. Also, the maximum temperature of outlet belongs to the $K = 1.25$ mm. It is clear that the difference between 1.25 mm and 1 mm is very small.

In Fig. 20, the contours of temperature are depicted on a plate in the middle of the channel for the different gaps between two consecutive convergent–divergent sections (K). Accordingly, it can be seen that the differences between the models in the contours here are not significant. However, $K = 1.25$ mm has the highest outlet temperature with low difference.

In Fig. 21, the contour of temperature is depicted in the outlet for different gaps between two consecutive convergent–divergent sections (K). The trend shown in Fig. 21 is the same with Fig. 20 and high outlet temperature belongs to the $K = 1.25$ mm.

The average Nusselt number (Nu) and the thermal performance (η) versus Reynolds number for different gaps between two consecutive convergent–divergent sections (K) are illustrated in Fig. 22a, b, respectively.

According to Fig. 22a, it can be seen that the average Nusselt number increases as the Reynolds number rises. Also, the maximum and minimum average Nusselt number (Nu) belong to the $K = 1.75$ mm and $K = 1$ mm, respectively. In Fig. 22b, the base case ($\eta = 1$) is the case with $k = 1.75$. According to Fig. 22b, as the gap between two consecutive convergent–divergent sections (K) decreases, the thermal performance declines. The maximum and minimum thermal performance belong to the $K = 1.75$ and $K = 1$, respectively.

The effect of using nanofluid

In this section, the effect of utilizing different types of water-based nanofluids, including Al_2O_3 and CuO on heat transfer enhancement in a convergent–divergent tube is investigated numerically. The simulations were performed for two values of φ (3 and 5%). Here, the geometrical parameters of considered tube, including D_1, D_2, P and K, were kept constant as 25, 16, 25 and 8 mm, respectively. The pressure drop and outlet temperature of various water-based nanofluid in comparison with pure water versus Reynolds number for $\varphi = 3$ and 5% are illustrated in Fig. 23a, b, respectively.

Figure 23a, b shows that the outlet temperature decreases as Reynolds number increases and the trend is
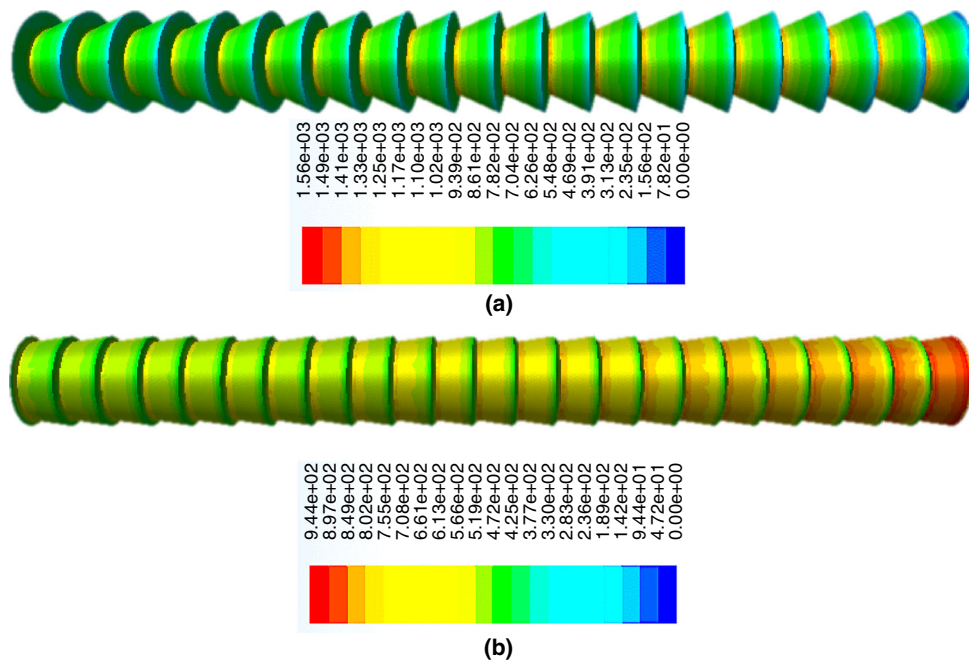
Fig. 14 3D contours of local Nusselt number for two different α_2 dimensionless geometrical parameters at $Re = 20,000$ **a** $\alpha_2 = 0.06$ and **b** $\alpha_2 = 0.09$
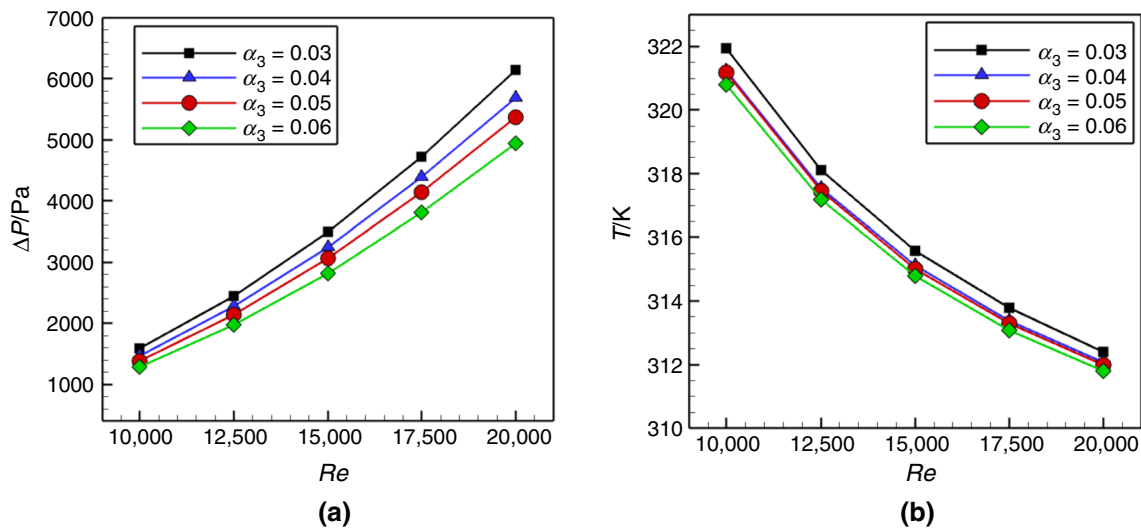

Fig. 15 **a** Output temperature of water and **b** pressure drop versus Reynolds number for different α_3 dimensionless parameters (different pitches of the convergent–divergent wall) at $D_1 = 16$ mm, $D_2 = 23$ mm and $K = 1.25$ mm

the same for all models. Also, the results indicate that the water-based nanofluids have higher outlet temperature in comparison with pure water. However, differences between the water/Al$_2$O$_3$ and water/CuO nanofluid are very low. As a result, it can be seen that water/Al$_2$O$_3$ nanofluid has higher outlet temperature (very low difference with water/CuO nanofluid).

Also, according to Fig. 23a, b, it can be seen that utilizing nanofluid leads to more pressure drop in comparison with pure water in both considered volume concentrations

of water-based nanofluid (3 and 5%). Between the two types of studied water-based nanofluid, water/CuO nanofluid has higher pressure drop than water/Al$_2$O$_3$ and the difference between them is higher in 5% in comparison with 3% volume concentration.

The average Nusselt number (Nu) and thermal performance (η) versus different Reynolds numbers (Re) for two types of water-based nanofluid are illustrated in Fig. 24. Two different volume concentrations of water-based nanofluid, including 3 and 5%, are considered here, and the
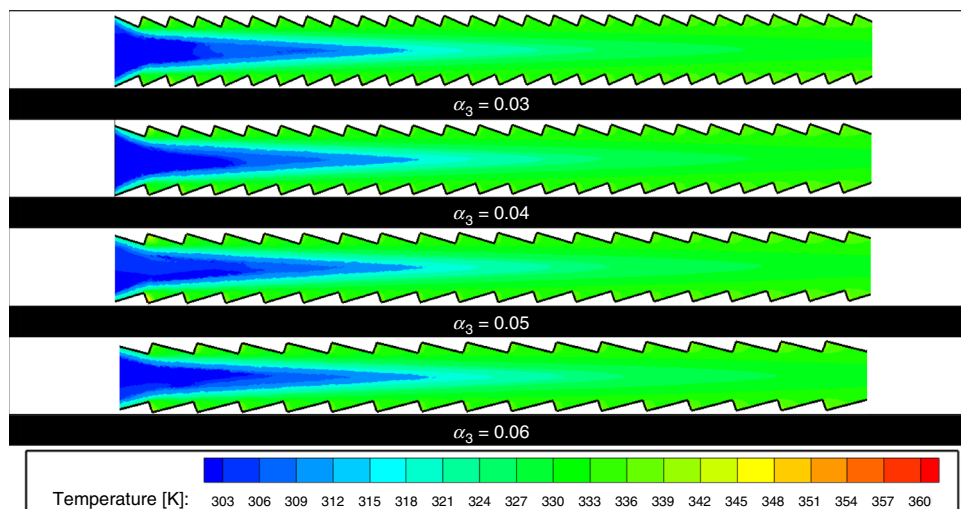
Fig. 16 The contours of temperature in the middle of the channel for different α_3 dimensionless parameters at $Re = 15{,}000$, $D_1 = 16$ mm, $D_2 = 23$ mm and $K = 1.25$ mm
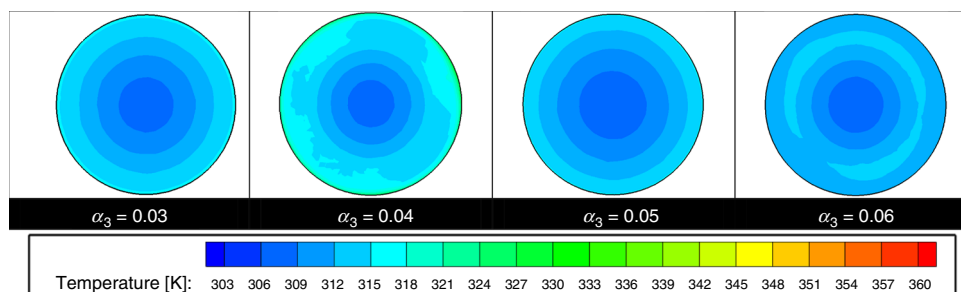

Fig. 17 Contours of temperature at the outlet of tube for different α_3 dimensionless parameters at $Re = 15{,}000$, $D_1 = 16$ mm, $D_2 = 23$ mm and $K = 1.25$ mm

obtained results for each of them are shown in Fig. 24a, b, respectively.

According to Fig. 20a, b, it can be realized that the average Nusselt number of water-based nanofluid is more than pure water in both volume concentrations (3 and 5%). Also, among the investigated water-based nanofluid, CuO has higher average Nusselt number in comparison with Al_2O_3 and the difference between them becomes higher in 5%. By increasing the Reynolds number, the average Nusselt number rises and the trend is the same for both of studied volume concentration of the water-based nanofluids.

By considering the thermal performance figures, it should be noted firstly that the base case ($\eta = 1$) belongs to the pure water. The thermal performances of the both studied water-based nanofluids are more than unity which means better than pure water. Also, Fig. 20b shows that as the volume concentration increases, the thermal performance rises in both nanofluids. As a result, CuO/water

nanofluid has better thermal performance than water/Al_2O_3 and especially pure water.

The effect of volume concentration of water-based nanofluid

In this section, the effect of volume concentration of two water-based nanofluids (Al_2O_3 and CuO) on the heat transfer rate and thermal performance is evaluated numerically. The geometrical parameters of the convergent–divergent tube including D_1, D_2, P and K are kept constant as 16, 25, 8 and 1.25 mm, respectively. Four different volume concentrations of water-based nanofluid, including 2, 3, 4 and 5%, are considered here. The simulations are performed for five different Reynolds numbers ($Re = 10{,}000$–$20{,}000$).

The pressure drop (ΔP) and the average temperature of the outlet for two types of water-based nanofluids, including water/Al_2O_3 and water/CuO, are shown in Fig. 25a, b, respectively. Accordingly, it can be seen that
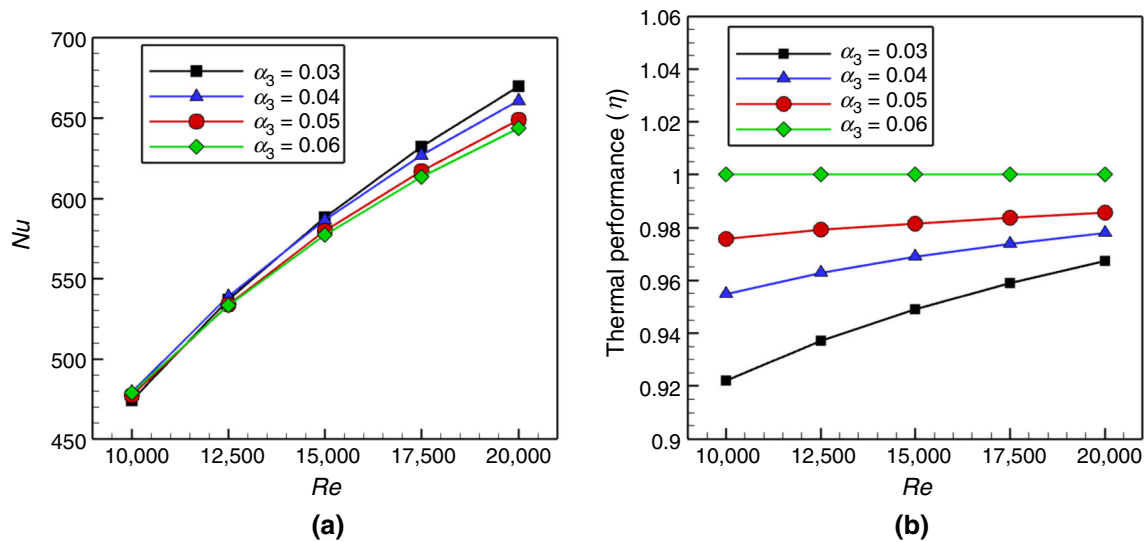
Fig. 18 **a** Average Nusselt number (*Nu*) and **b** thermal performance (*η*) versus Reynolds number for different α_3 dimensionless parameters (different pitches of the convergent–divergent wall) at $D_1 = 16$ mm, $D_2 = 23$ mm and $K = 1.25$ mm
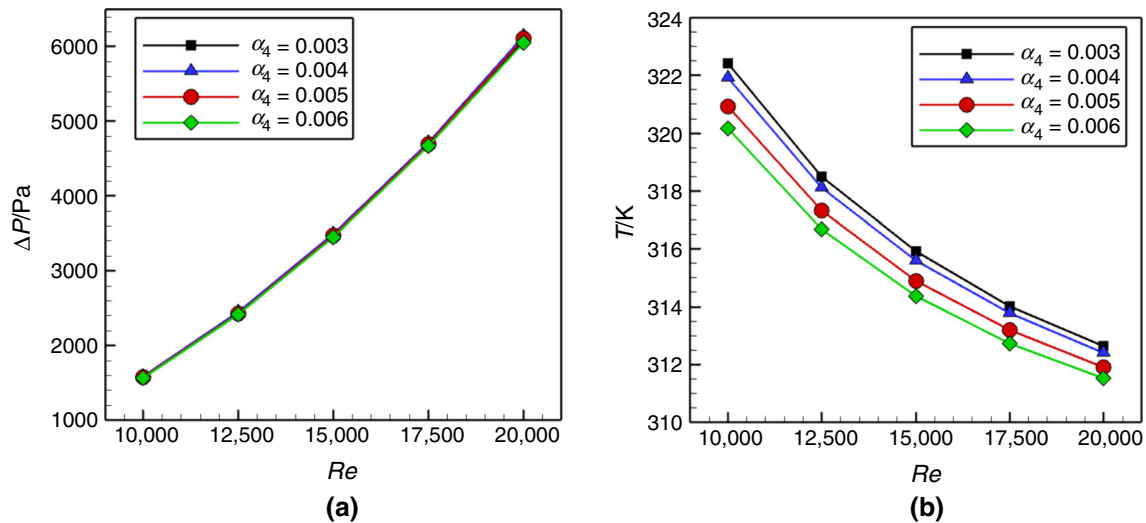

Fig. 19 **a** Output temperature of water and **b** pressure drop versus different Reynolds numbers and various gap between two consecutive convergent–divergent sections for different α_3 dimensionless parameters (different pitches of the convergent–divergent wall) at $D_1 = 16$ mm, $D_2 = 23$ mm and $P = 8$ mm

high pressure drop belongs to higher volume concentration of nanofluid and it is clear more for water/CuO tan water/Al_2O_3. For outlet temperature, there is no significant difference between the various considered volume concentrations. However, $\varphi = 5\%$ and $\varphi = 2\%$ have maximum and minimum outlet temperatures, respectively, with very low difference. (The present results are the same for both types of nanofluids.)

The heat transfer coefficient (*h*) and thermal performance (*η*) versus different Reynolds numbers (*Re*) for various volume concentrations of water-based nanofluid and two different types of water-based nanofluids (Al_2O_3 and CuO) are illustrated in Fig. 26a, b, respectively.

Accordingly, it can be seen that the higher volume concentration of water-based nanofluid leads to higher heat transfer coefficient. The base model for thermal performance figure is pure water ($\eta = 1$).

According to Fig. 26a, b, as the Reynolds number increases, the heat transfer coefficient rises which the trend is the same for both nanofluids however, the values of heat transfer coefficient of water/CuO nanofluid is a little more than water/Al_2O_3. Also, the volume concentration of nanofluid rises leading to growth in heat transfer coefficient. It should be noted that the differences between the cases with different volume concentrations for water/Al_2O_3 are lower than water/CuO.
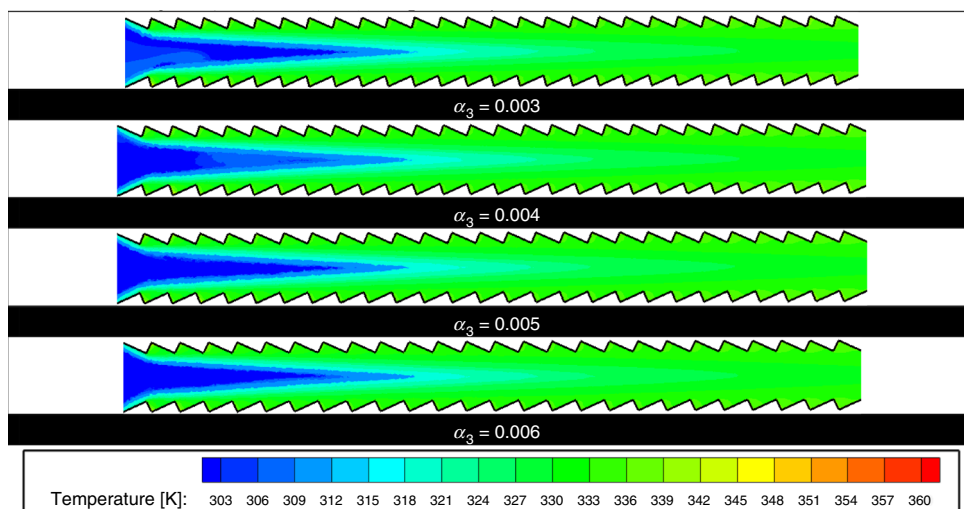
Fig. 20 The contours of temperature in the middle of the channel for different α_3 dimensionless parameters (different pitches of the convergent–divergent wall) at $Re = 15,000$, $D_1 = 16$ mm, $D_2 = 23$ mm and $P = 8$ mm
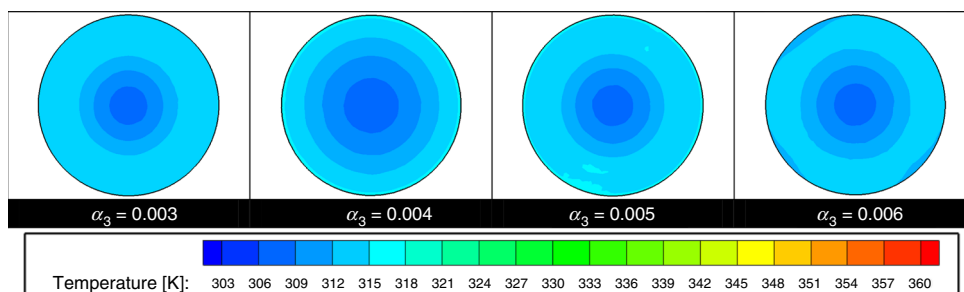

Fig. 21 Contours of temperature at the outlet of tube for different α_3 dimensionless parameters (different pitches of the convergent–divergent wall) at $Re = 15,000$, $D_1 = 16$ mm, $D_2 = 23$ mm and $P = 8$ mm

As the Reynolds number rises, the thermal performance declines which the trend is the same for both nanofluid. Also, the values of thermal performance of water/Al_2O_3 are more than water/CuO. Also, by rising the volume concentration (from 2 to 5%) for water/Al_2O_3, the highest and lowest thermal performances belong to $\varphi = 5\%$ and 2%, respectively. It is clearly shown that utilizing nanofluid with any volume concentration (2–5%) has better thermal performance significantly in comparison with pure water for both nanofluid.

However, the trend of the profile of thermal performance for water/CuO nanofluid is different with the water/Al_2O_3 nanofluid. For water/CuO nanofluid, the highest and lowest thermal performances belong to $\varphi = 3$ and 5%, respectively. Also, it is shown that the effect of the volume concentration of water-based nanofluid at low Reynolds number is more than higher one.

As a result, it can be said that for water/Al_2O_3 nanofluid at low Reynolds number ($Re = 10,000$), the case with $\varphi = 4\%$ has 9.29% more thermal performance than pure water which has the highest thermal performance. Also, at high Reynolds number ($Re = 20,000$), the case with $\varphi = 5\%$ has 7.15% more thermal performance than pure water. The lowest thermal performance improvement in comparison with pure water belongs to the case with $\varphi = 2\%$ at high Reynolds number ($Re = 20,000$) with about 6%.

Also, for water/CuO nanofluid, the case with $\varphi = 3\%$ at low Reynolds number ($Re = 10,000$) and the case with $\varphi = 5\%$ at high Reynolds number ($Re = 20,000$) have highest and lowest thermal performance improvement in comparison with pure water with 8.86% and 6.25%, respectively.

Conclusions

In the present study, the heat transfer and fluid flow of water-based nanofluid in the convergent–divergent tube were evaluated numerically. The simulations were
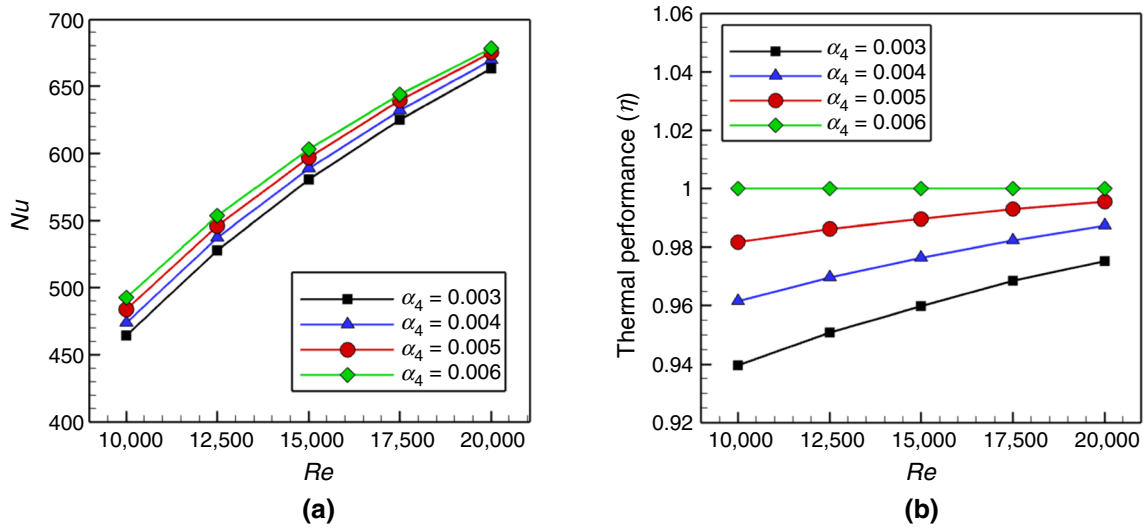
Fig. 22 a Average Nusselt number (*Nu*) and **b** thermal performance (*η*) versus Reynolds number for different α_3 dimensionless parameters (different pitches of the convergent–divergent wall) at $D_1 = 16$ mm, $D_2 = 23$ mm and $P = 8$ mm

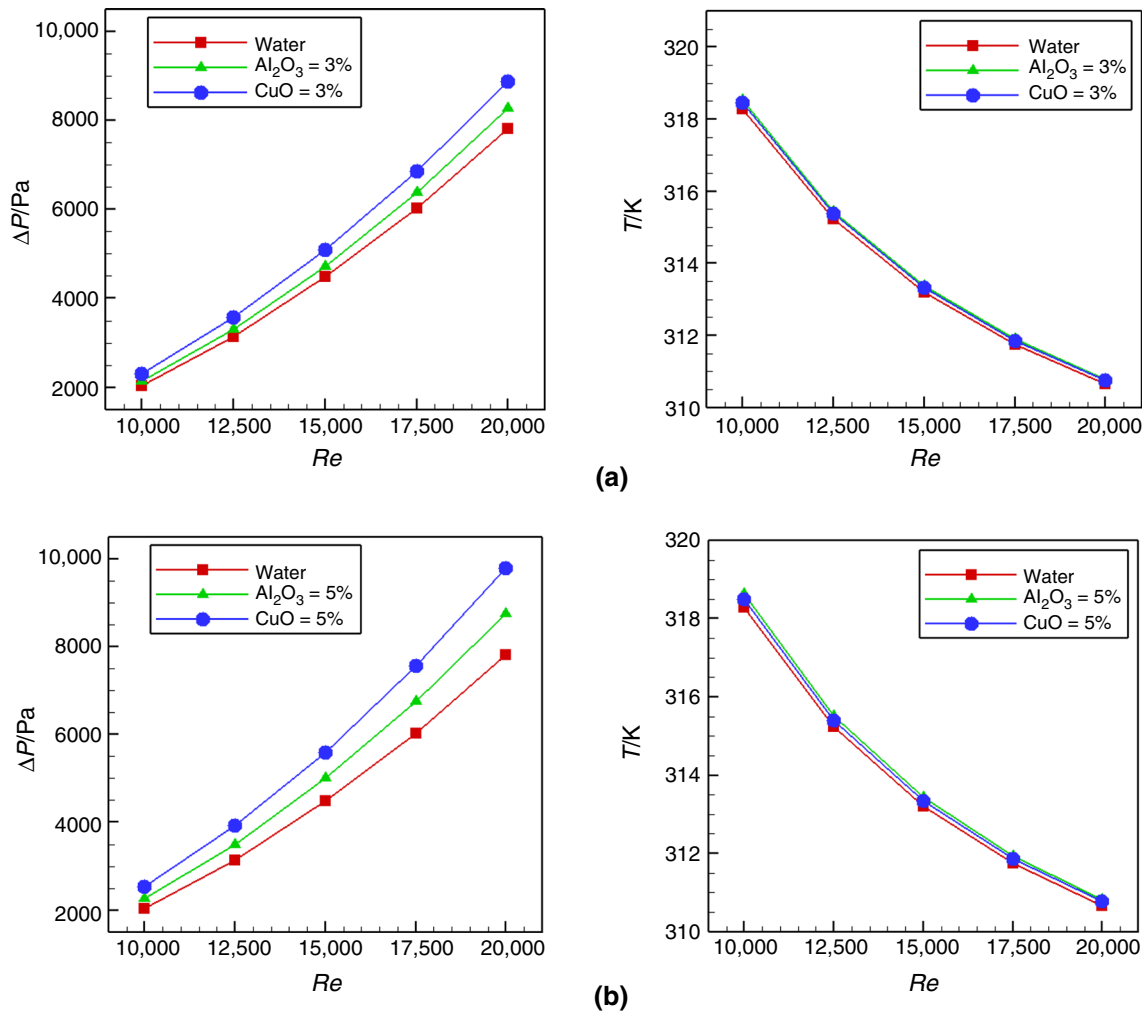**Fig. 23** Pressure drop (*ΔP*) and temperature of the outlet versus different Reynolds numbers for various water-based nanofluids and pure water **a** $\varphi = 3\%$ and **b** $\varphi = 5\%$
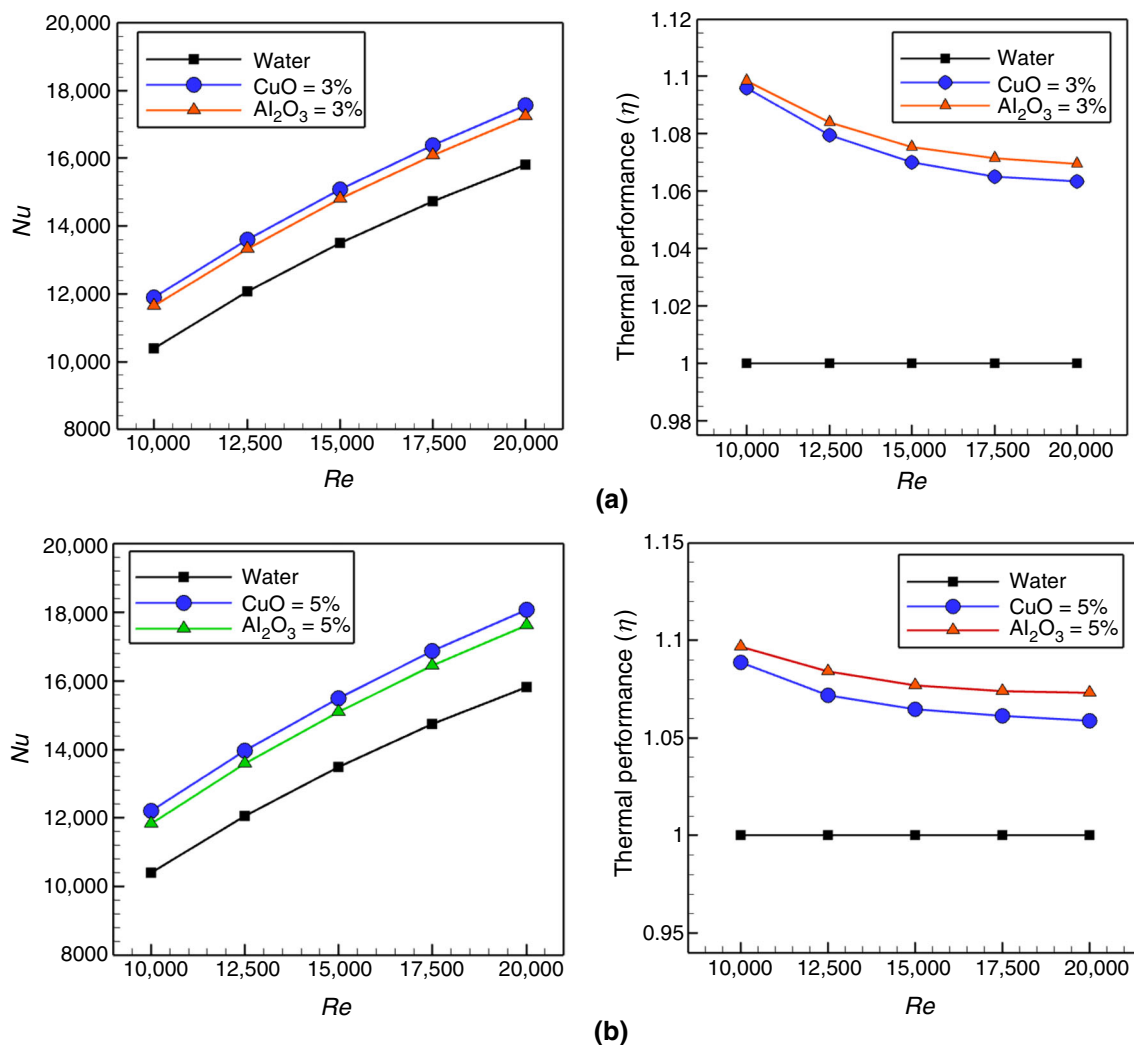
Fig. 24 Average Nusselt number (*Nu*) and thermal performance (η) versus different Reynolds numbers for various water-based nanofluids and pure water **a** $\varphi = 3\%$ and **b** $\varphi = 5\%$

performed by a commercial CFD coed, ANSYS FLUENT 18.2. The present paper includes two sections, which at the first section, the effects of geometrical and operational parameters on the thermal performance of the convergent–divergent tube were studied. The geometrical parameters include the large diameter of the cone's wall, the small diameter of the cone's wall, pitch of the cone and the height of the roughness. The utilized fluid in this section was pure water. At the second section, two different types of water-based nanofluids, including water/Al_2O_3 and water/CuO, are considered and the obtained results were compared with the pure water. Also, the effect of volume concentration of nanofluid was analyzed numerically. Obtained results are as follows:

- The growth of large diameter of the cone leads to better temperature uniformity, or better heat transfer between

the wall and the fluid occurs. Therefore, it can be concluded that the large diameter increase will have a significant effect on the temperature of the water output from the converter.

- As small diameter of the cone increases, the average Nusselt number (*Nu*) declines. Also, lowest small diameter of the cone leads to higher thermal performance (high heat transfer rate with low pressure drop).

- As the pitch of the convergent–divergent wall rises, the average Nusselt number decreases. Highest thermal performance is achieved for the lowest value of the pitch.

- The thermal performances of the both studied water-based nanofluids are more than unity which means better than pure water. Water/Al_2O_3 nanofluid has
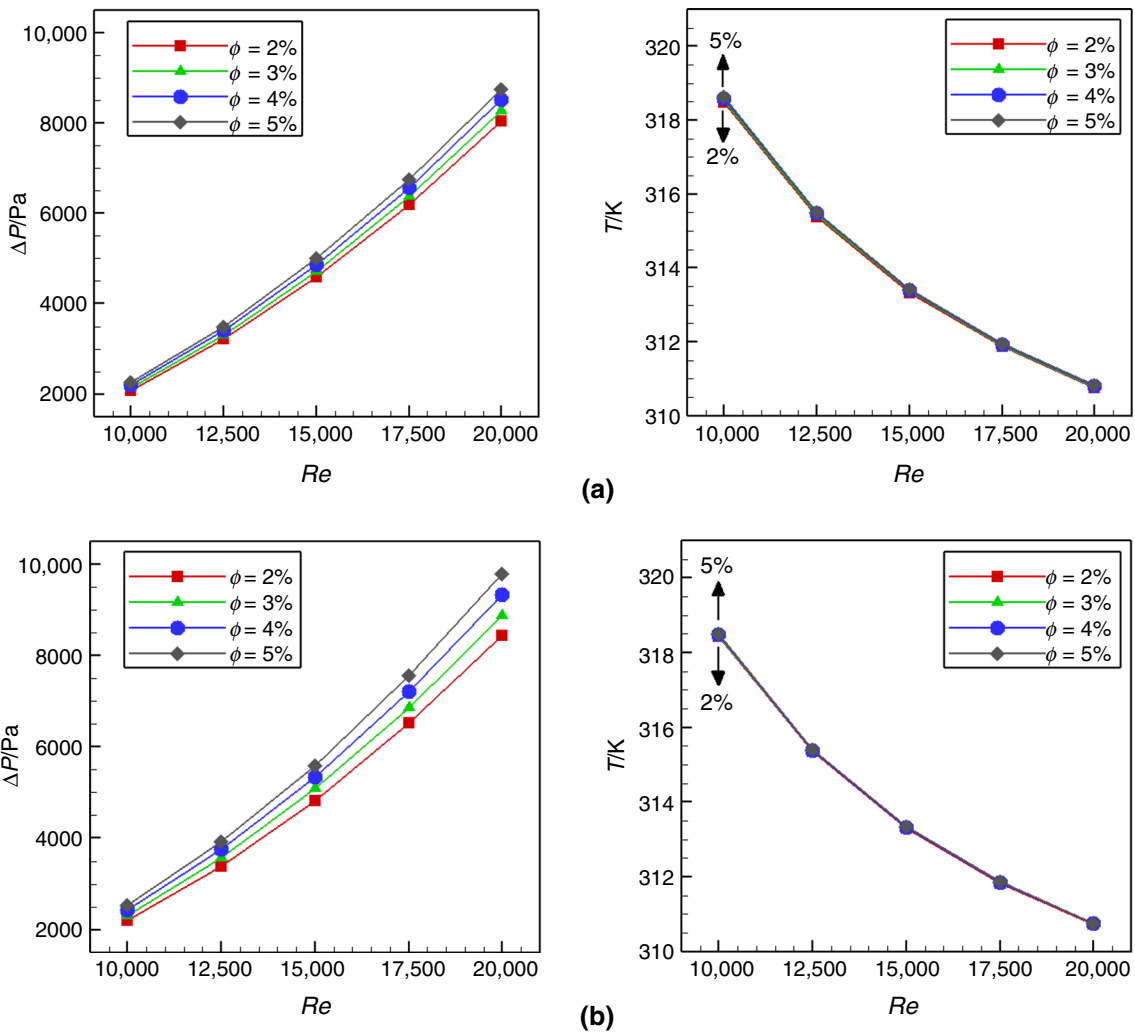
Fig. 25 Pressure drop (ΔP) and temperature of outlet versus different Reynolds numbers for various volume concentration of nanofluid **a** water/Al$_2$O$_3$ and **b** water/CuO

better thermal performance than CuO/water and especially pure water.

- As a result, it can be said that for water/Al$_2$O$_3$ nanofluid at low Reynolds number ($Re = 10,000$), the case with $\varphi = 4\%$ has 9.29% more thermal performance than pure water which has the highest thermal performance. Also, at high Reynolds number ($Re = 20,000$), the case with $\varphi = 5\%$ has 7.15% more thermal performance than pure water. The lowest thermal performance improvement in comparison with pure water belongs to the case with $\varphi = 2\%$ at high Reynolds number

($Re = 20,000$) with about 6%. Also, for water/CuO nanofluid, the case with $\varphi = 3\%$ at low Reynolds number ($Re = 10,000$) and the case with $\varphi = 5\%$ at high Reynolds number ($Re = 20,000$) have highest and lowest thermal performance improvement in comparison with pure water with 8.86% and 6.25%, respectively.
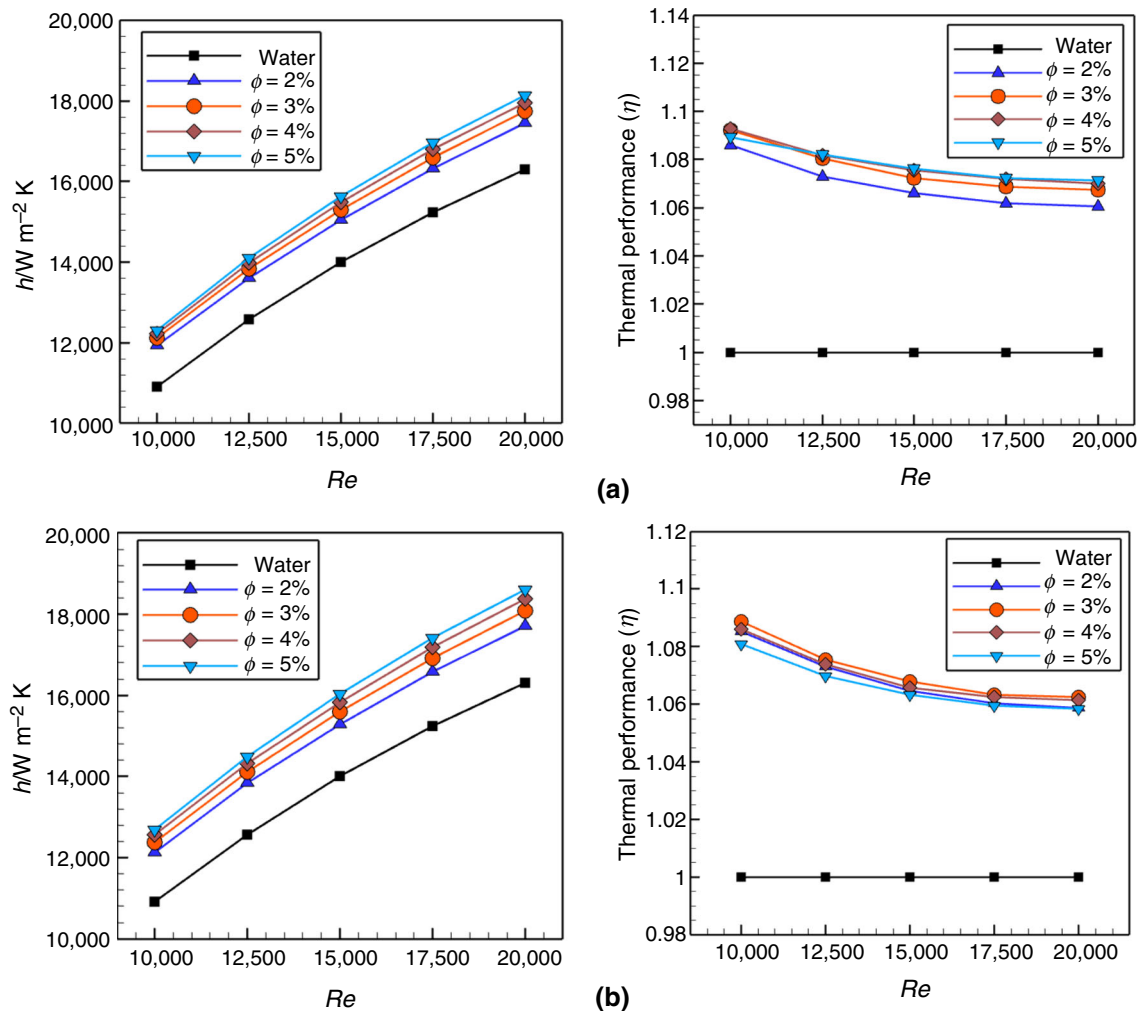
Fig. 26 Heat transfer coefficient (h) and thermal performance (η) versus different Reynolds numbers for various volume concentration of nanofluid **a** water/Al$_2$O$_3$ and **b** water/CuO

References

1. Rainieri S, Pagliarini G. Convective heat transfer to temperature dependent property fluids in the entry region of corrugated tubes. Int J Heat Mass Transf. 2002;45(22):4525–36.

2. Promvonge P, Eiamsa-ard S. Heat transfer behaviors in a tube with combined conical-ring and twisted-tape insert. Int Commun Heat Mass Transfer. 2007;34:849–59.

3. Garcia A, Solano JP, Vicente PG, Viedma A. The influence of artificial roughness shape on heat transfer enhancement: corrugated tubes, dimpled tubes and wire coils. Appl Therm Eng. 2012;35:196–201.

4. Eiamsa-ard S, Yongsiri K, Nanan K, Thianpong C. Heat transfer augmentation by helically twisted tapes as swirl and turbulence promoters. Chem Eng Process. 2012;60:42–8.

5. Darzi AAR, Farhadi M, Sedighi K, Aallahyari SH, Delavar MA. Turbulent heat transfer of Al$_2$O$_3$–water nanofluid inside helically corrugated tubes: numerical study. Int Commun Heat Mass Transfer. 2013;41:68–75.

6. Mohammadi K, Sabzpooshani M. Comprehensive performance evaluation and parametric studies of single pass solar air heater with fins and baffles attached over the absorber plate. Energy. 2013;57:741–50.

7. Naik MT, Fahad SS, Sundar LS, Singh MK. Comparative study on thermal performance of twisted tape and wire coil inserts in turbulent flow using CuO/water nanofluid. Exp Thermal Fluid Sci. 2014;57:65–76.

8. Esmaeilzadeh E, Almohammadi H, Nokhosteen A, Motezaker A, Omrani AN. Study on heat transfer and friction factor characteristics of g-Al$_2$O$_3$/water through circular tube with twisted tape inserts with different thicknesses. Int J Therm Sci. 2014;82:72–83.

9. Zohir AE, Aziz AAA, Habib MA. Heat transfer characteristics and pressure drop of the concentric tube equipped with coiled wires for pulsating turbulent flow. Exp Thermal Fluid Sci. 2015;65:41–51.

10. Kareem ZS, Abdullah S, Lazim TM, MohdJaafar MN, Wahid AFA. Heat transfer enhancement in three-start spirally corrugated tube: experimental and numerical study. Chem Eng Sci. 2015;134:746–57.

11. Bhuiya MMK, Azad AK, Chowdhury MSU, Saha M. Heat transfer augmentation in a circular tube with perforated double counter twisted tape inserts. Int Commun Heat Mass Transfer. 2016;74:18–26.

12. Afsharpanah F, Pakzad K, Amirsoleymani M, Delavar MA. Numerical study of heat transfer enhancement using perforated

dual twisted tape inserts in converging–diverging tubes. Heat Transf Asian Res. 2018;47(5):754–67.

13. Nakhchi ME, Esfahani JA. Entropy generation of turbulent Cu–water nanofluid flow in a heat exchanger tube fitted with perforated conical rings. J Therm Anal Calorim 2019. https://doi.org/10.1007/s10973-019-08169-w.

14. Toghraie D, Abdollah MM, Pourfattah F, Akbari OA, Ruhani B. Numerical investigation of flow and heat transfer characteristics in smooth, sinusoidal and zigzag-shaped microchannel with and without nanofluid. J Therm Anal Calorim. 2018;131(2):1757–66.

15. Bhattacharyya S, Pal SK, Pop I. Impact of nanoparticles migration on mixed convection and entropy generation of a Al_2O_3–water nanofluid inside an inclined enclosure with wavy side wall. J Therm Anal Calorim 2019. https://doi.org/10.1007/s10973-019-08345-y.

16. Mohebbi R, Izadi M, Delouei AA, Sajjadi H. Effect of MWCNT–Fe_3O_4/water hybrid nanofluid on the thermal performance of ribbed channel with apart sections of heating and cooling. J Therm Anal Calorim. 2019;135(6):3029–42.

17. Sajid MU, Ali HM, Sufyan A, Rashid D, Zahid SU, Rehman WU. Experimental investigation of TiO_2–water nanofluid flow and heat transfer inside wavy mini-channel heat sinks. J Therm Anal Calorim. 2019;137(4):1279–94.

18. Kuppusamy NR, Mohammed HA, Lim CW. Numerical investigation of trapezoidal grooved microchannel heat sink using nanofluids. Thermochim Acta. 2013;573:39–56.

19. Kuppusamy NR, Mohammed HA, Lim CW. Thermal and hydraulic characteristics of nanofluid in a triangular grooved microchannel heat sink (TGMCHS). Appl Math Comput. 2014;246:168–83.

20. Mohammed HA, Narrein K. Thermal and hydraulic characteristics of nanofluid flow in a helically coiled tube heat exchanger. Int Commun Heat Mass Transfer. 2012;39(9):1375–83.

21. Narrein K, Mohammed HA. Influence of nanofluids and rotation on helically coiled tube heat exchanger performance. Thermochim Acta. 2013;564:13–23.

22. Mohammed HA, Golieskardi M, Munisamy KM. Numerical investigation of combined convection and nanofluids flow over backward facing step in a channel having a blockage. J Comput Theor Nanosci. 2014;11(4):971–80.

23. Fluent AN. 18.2, theory guide. Canonsburg: ANSYS Inc.; 2017.

24. Shih TH, Liou WW, Shabbir A, Yang Z, Zhu J. A new k–ε Eddy viscosity model for high reynolds number turbulent flows. Comput Fluids. 1995;24:227–38.

25. Xuan Y, Roetzel W. Conceptions for heat transfer correlation of nanofluids. Int J Heat Mass Transf. 2000;43(19):3701–7.

26. Piper M, Tran JM, Kenig EY. A CFD study of the thermo-hydraulic characteristics of pillow-plate heat exchangers. In: ASME 2016 heat transfer summer conference collocated with the ASME 2016 fluids engineering division summer meeting and the ASME 2016 14th international conference on nanochannels, microchannels, and minichannels. American Society of Mechanical Engineers; 2016. pp. V001T05A002.

27. Corcione M. Empirical correlating equations for predicting the effective thermal conductivity and dynamic viscosity of nanofluids. Energy Convers Manag. 2011;52(1):789–93.

28. Pak BC, Cho YI. Hydrodynamic and heat transfer study of dispersed fluids with submicron metallic oxide particles. Exp Heat Transf Int J. 1998;11(2):151–70.

29. Sharma KV, Sarma PK, Azmi WH, Mamat R, Kadirgama K. Correlations to predict friction and forced convection heat transfer coefficients of water based nanofluids for turbulent flow in a tube. Int J Microscale Nanoscale Therm Fluid Transp Phenom. 2012;3(4):283.

30. Fotukian SM, Esfahany MN. Experimental study of turbulent convective heat transfer and pressure drop of dilute CuO/water nanofluid inside a circular tube. Int Commun Heat Mass Transfer. 2010;37(2):214–9.

31. Baragh S, Shokouhmand H, Ajarostaghi SS, Nikian M. An experimental investigation on forced convection heat transfer of single-phase flow in a channel with different arrangements of porous media. Int J Therm Sci. 2018;1(134):370–9.

32. Ko KH, Anand NK. Use of porous baffles to enhance heat transfer in a rectangular channel. Int J Heat Mass Transf. 2003;46(22):4191–9.

33. Chang SW, Liou TM, Chiang KF, Hong GF. Heat transfer and pressure drop in rectangular channel with compound roughness of V-shaped ribs and deepened scales. Int J Heat Mass Transf. 2008;51:457–68.

34. Kurtbaş İ, Gülçimen F, Akbulut A, Buran D. Heat transfer augmentation by swirl generators inserted into a tube with constant heat flux. Int Commun Heat Mass Transfer. 2009;36(8):865–71.

35. Baragh S, Shokouhmand H, Ajarostaghi SSM. Experiments on mist flow and heat transfer in a tube fitted with porous media. Int J Therm Sci. 2019;137:388–98.

36. Noorbakhsh M, Zaboli M, Ajarostaghi SS. Numerical evaluation of the effect of using twisted tapes as turbulator with various geometries in both sides of a double-pipe heat exchanger. J Therm Anal Calorim 2019. https://doi.org/10.1007/s10973-019-08509-w.

37. Shirzad M, Delavar MA, Ajarostaghi SSM, Sedighi K. Evaluation the effects of geometrical parameters on the performance of pillow plate heat exchanger. Chem Eng Res Des. 2019;150:74–83.

38. Shirzad M, Ajarostaghi SSM, Delavar MA, Sedighi K. Improve the thermal performance of the pillow plate heat exchanger by using nanofluid: numerical simulation. Adv Powder Technol. 2019;30(7):1356–65.